

The Gildener-Weinberg two-Higgs doublet model at two loops*

Estia J. Eichten^{1†} and Kenneth Lane^{2‡}

¹Theoretical Physics Group, Fermi National Accelerator Laboratory
P.O. Box 500, Batavia, Illinois 60510

²Department of Physics, Boston University
590 Commonwealth Avenue, Boston, Massachusetts 02215

September 21, 2022

Abstract

The Gildener-Weinberg two-Higgs doublet model (GW-2HDM) provides a naturally light and aligned Higgs boson, $H = H(125)$. It has been studied in the one-loop approximation of its effective potential, V_1 . An important consequence is that the masses of the model's BSM Higgs bosons (H', A, H^\pm) are bounded by the sum rule $(M_{H'}^4 + M_A^4 + 2M_{H^\pm}^4)^{1/4} = 540 \text{ GeV}$. Although they are well within reach of the LHC, searches for them have been stymied by large QCD backgrounds. Another consequence is that H is highly aligned, i.e., H - H' mixing is small and H has only Standard Model couplings. A corollary of this alignment is that search modes such as $H', A \leftrightarrow W^+W^-, ZZ, HZ$ and $H^\pm \leftrightarrow W^\pm Z, W^\pm H$ are greatly suppressed. To assess the accuracy of the sum rule and Higgs alignment, we study this model in two loops. This calculation is complicated by having many new contributions. We present two formulations of it to calculate the H - H' mass matrix, its eigenvectors H_1, H_2 , and the mass M_{H_2} while fixing $M_{H_1} = 125 \text{ GeV}$. They give similar results, in accord with the one-loop results. Requiring $M_A = M_{H^\pm}$, we find $180 \text{ GeV} \lesssim M_{A, H^\pm} \lesssim 380\text{--}425 \text{ GeV}$ and $550\text{--}700 \text{ GeV} \gtrsim M_{H_2} \gtrsim 125 \text{ GeV}$, with M_{H_2} decreasing as M_{A, H^\pm} increase. The corrections to H -alignment are below $\mathcal{O}(1\%)$. So, the BSM searches above will remain fruitless. Finding the BSM Higgses requires improved sensitivity to their low masses. We discuss two possible searches for this.

*This paper is dedicated to Kurt Gottfried and Eric Pilon, our friends and collaborators.

†eichten@fnal.gov

‡lane@bu.edu

I. Review and Overview

In the Gildener-Weinberg (GW) scheme of electroweak symmetry breaking in multi-Higgs multiplet models, the scalar potential $V_0(\Phi_i)$ of the tree-level Lagrangian consists of only quartic interaction terms [1]. Therefore, so long as all particle masses arise from the vacuum expectation values (VEVs) $\langle\phi_i\rangle$ of Φ_i , the theory is classically scale-invariant. This happens if the linear combination of Φ_i that is the Higgs boson, H , is also a Goldstone boson of spontaneous breaking of this scale invariance, the dilaton of a flat minimum of V_0 along a ray $0 < \phi < \infty$ in field space.

Because it is such a Goldstone boson, H is the same form of linear combination of scalars as the Goldstone bosons eaten by W^\pm and Z ; that is, in an N -multiplet model,

$$H = \sum_{i=1}^N (\langle\phi_i\rangle/\phi)\phi_i \quad (1)$$

where $\sqrt{\sum_i \langle\phi_i\rangle^2} = \phi$. This is important: this Higgs boson is perfectly aligned, that is, it has exactly the same couplings to gauge bosons and fermions as the Standard Model (SM) Higgs [2, 3, 4, 5, 6]. While it is massless at tree-level, the Higgs gets a mass at the one-loop level of the Coleman-Weinberg effective potential, V_1 [7]. The renormalization scale in V_1 explicitly breaks the scale symmetry of V_0 , inducing a minimum of $V_0 + V_1$ that picks out a specific value v of ϕ . This v is identified as the weak scale, 246 GeV, and it sets the scale of all masses in the theory.¹ As we review in this section, the one-loop corrections to perfect alignment are very small, typically $\lesssim \mathcal{O}(1\%)$ *in amplitude*. Thus, the approximate scale symmetry of GW models makes the Higgs *naturally light and aligned* [8].

This naturalness requires no symmetry other than scale invariance. Therefore, in GW models there are no partners, scalar or fermionic, of the top quark, of the weak bosons, nor of any other particles except for the additional scalars occurring in multi-Higgs multiplet models. Nor are there the vectorial fermions requiring tree-level bare masses. The GW scheme is the only one we know in which the same agent, the Higgs VEV v , is responsible

¹For economy of narrative, we are ignoring here the spontaneous breaking of the light quarks' chiral symmetry that sets the mass scale of the light hadrons.

for electroweak symmetry breaking and for explicit scale symmetry breaking. Hence, the “dilaton scale” f is *equal* to v [9]. The one sure way to test these models is to search for the additional Higgs scalars [10, 11]. They are exceptionally light, with masses below about 400–550 GeV in one-loop order. We review this calculation below in a two-Higgs-doublet model. This model has three Beyond-Standard-Model Higgs (BSM) bosons, a CP -even H' , a CP -odd A and a singly-charged H^\pm (see the standard Ref. [12] for details).

To evaluate the robustness of the one-loop predictions, we extend their calculation to the two-loop effective potential [13]. This is considerably more complicated than in one loop. Therefore, in Secs. II and III we present two methods of calculating the two-loop contributions to the CP -even mass-squared matrix, \mathcal{M}_{0+}^2 , as a function of BSM Higgs masses $M_A = M_{H^\pm}$ and $M_{H'}$.² The two methods give qualitatively similar results and, so, support the low bound on the masses of the new Higgs scalars and our earlier conclusion on the degree of the 125-GeV Higgs boson’s alignment. To our knowledge, two-loop calculations of Gildener-Weinberg multi-Higgs models have not been carried out in this depth. The experimental consequences of our calculations, including the impact of ATLAS and CMS searches relevant to the model’s BSM Higgs bosons, are presented in Sec. IV. Readers interested mainly in these consequences can skip to Sec. IV.

The simplest model employing the GW mechanism is the two-Higgs doublet model (2HDM) proposed by Lee and Pilaftsis in 2012 [16]. The tree-level potential of the two doublets is

$$\begin{aligned}
 V_0(\Phi_1, \Phi_2) &= \lambda_1(\Phi_1^\dagger\Phi_1)^2 + \lambda_2(\Phi_2^\dagger\Phi_2)^2 + \lambda_3(\Phi_1^\dagger\Phi_1)(\Phi_2^\dagger\Phi_2) \\
 &+ \lambda_4(\Phi_1^\dagger\Phi_2)(\Phi_2^\dagger\Phi_1) + \frac{1}{2}\lambda_5\left((\Phi_1^\dagger\Phi_2)^2 + (\Phi_2^\dagger\Phi_1)^2\right), \quad (2)
 \end{aligned}$$

where the doublets are

$$\Phi_i = \frac{1}{\sqrt{2}} \begin{pmatrix} \sqrt{2}\phi_i^+ \\ \rho_i + ia_i \end{pmatrix}, \quad i = 1, 2, \quad (3)$$

and ρ_i and a_i are neutral CP -even and odd fields. The five quartic coup-

²The constraint $M_A = M_{H^\pm}$ is motivated by the fact that it makes the contribution to the T -parameter from the BSM scalars vanish [14, 15, 16].

lings λ_i in Eq. (2) are real and V_0 is CP -invariant.³ Positivity of V_0 requires that $\lambda_1, \lambda_2 > 0$, This potential is consistent with a \mathcal{Z}_2 symmetry that prevents tree-level flavor-changing interactions among fermions, ψ , induced by neutral scalar exchange [17]. We define this \mathcal{Z}_2 to be

$$\Phi_1 \rightarrow -\Phi_1, \quad \Phi_2 \rightarrow \Phi_2, \quad \psi_L \rightarrow -\psi_L, \quad \psi_{uR} \rightarrow \psi_{uR}, \quad \psi_{dR} \rightarrow \psi_{dR}. \quad (4)$$

This is the usual type-I 2HDM [12], but with Φ_1 and Φ_2 interchanged. The net effect of this is that the experimental upper limit on $\tan\beta = v_2/v_1$ found for this theoretical model [8] is to be compared to experimental upper limits on $\cot\beta$ for this and the other three types of 2HDM's with natural flavor conservation.⁴We refer to this model as the GW-2HDM. This type-I coupling was imposed on the model in 2018 to make it consistent with precision electroweak measurements at LEP, searches for $t \rightarrow H^+b$ at the Tevatron [18] and the then-current LHC data. The most stringent constraints came from CMS [19] and ATLAS [20] searches for charged Higgs decay into $t\bar{b}$. Consistency with these searches required $\tan\beta \lesssim 0.50$ for $180 \text{ GeV} < M_{H^\pm} \lesssim 500 \text{ GeV}$. This limit on $\tan\beta$ was affirmed in Refs. [10, 11].

The trivial minimum of V_0 occurs at $\Phi_1 = \Phi_2 = 0$. But a nontrivial flat minimum of V_0 can occur on the ray $0 < \phi < \infty$:

$$\Phi_{1\beta} = \frac{1}{\sqrt{2}} \begin{pmatrix} 0 \\ \phi c_\beta \end{pmatrix}, \quad \Phi_{2\beta} = \frac{1}{\sqrt{2}} \begin{pmatrix} 0 \\ \phi s_\beta \end{pmatrix}, \quad (5)$$

where $c_\beta = \cos\beta$ and $s_\beta = \sin\beta$ and $\beta \neq 0, \pi/2$ is a fixed angle. The tree-level extremal conditions for this ray are

$$\begin{aligned} \left. \frac{\partial V_0}{\partial \rho_1} \right|_{\langle \rho_i \rangle} &= \phi^3 c_\beta (\lambda_1 c_\beta^2 + \frac{1}{2} \lambda_{345} s_\beta^2) = 0, \\ \left. \frac{\partial V_0}{\partial \rho_2} \right|_{\langle \rho_i \rangle} &= \phi^3 s_\beta (\lambda_2 s_\beta^2 + \frac{1}{2} \lambda_{345} c_\beta^2) = 0, \end{aligned} \quad (6)$$

where $\lambda_{345} = \lambda_3 + \lambda_4 + \lambda_5$. It can be proved that $V_0(\Phi_{i\beta}) = 0$ and, in fact, that any such purely quartic potential as well as its first derivative vanish at

³Of course, there is CP violation in the CKM matrix, but that has negligible effect on our study and we ignore it.

⁴Strictly speaking, in this 2HDM, the VEVs v_1 and v_2 of Φ_1 and Φ_2 have meaning only after scale invariance is explicitly broken and ϕ in Eq. (5) has a specific value.

any extremum [10]. These conditions on the quartic couplings,

$$\lambda_1 = -\frac{1}{2}\lambda_{345} \tan^2 \beta, \quad \lambda_2 = -\frac{1}{2}\lambda_{345} \cot^2 \beta, \quad (7)$$

remain true and in force *in all orders* of the loop expansion for the effective potential [1]. This will be important in our subsequent development.

The eigenvectors and eigenvalues of the scalars' squared “mass” matrices in tree approximation are given by

$$\begin{aligned} \begin{pmatrix} z \\ A \end{pmatrix} &= \begin{pmatrix} c_\beta & s_\beta \\ -s_\beta & c_\beta \end{pmatrix} \begin{pmatrix} a_1 \\ a_2 \end{pmatrix}, \quad M_z^2 = 0, \quad M_A^2 = -\lambda_5 \phi^2; \\ \begin{pmatrix} w^\pm \\ H^\pm \end{pmatrix} &= \begin{pmatrix} c_\beta & s_\beta \\ -s_\beta & c_\beta \end{pmatrix} \begin{pmatrix} \phi_1^\pm \\ \phi_2^\pm \end{pmatrix}, \quad M_{w^\pm}^2 = 0, \quad M_{H^\pm}^2 = -\frac{1}{2}\lambda_{45} \phi^2; \\ \begin{pmatrix} H \\ H' \end{pmatrix} &= \begin{pmatrix} c_\beta & s_\beta \\ -s_\beta & c_\beta \end{pmatrix} \begin{pmatrix} \rho_1 \\ \rho_2 \end{pmatrix}, \quad M_H^2 = 0, \quad M_{H'}^2 = -\lambda_{345} \phi^2. \end{aligned} \quad (8)$$

It is important to note that the extremal conditions (6) are equivalent to the vanishing of the Goldstone boson masses, M_z and M_{w^\pm} . The ray (5) is a (flat) minimum, with $V_0 = 0$, so long as the M^2 are non-negative, i.e., that $\lambda_5, \lambda_{45} = \lambda_4 + \lambda_5$ and λ_{345} are negative. The CP -even scalar H is the dilaton and, as discussed above, it is the same linear combination of fields as z and w^\pm are; i.e., H is aligned. Alignment will be modified in higher orders, but only slightly.

At this point and for our discussion of this model beyond the tree approximation, it is convenient to use the “aligned basis” of the Higgs fields because, in the GW-2HDM, H is very nearly aligned and separated from the BSM Higgs fields H', A, H^\pm *through two-loop order* in this basis.⁵ The aligned basis is:

$$\begin{aligned} \Phi &= \Phi_1 c_\beta + \Phi_2 s_\beta = \frac{1}{\sqrt{2}} \begin{pmatrix} \sqrt{2} w^+ \\ H + iz \end{pmatrix}, \\ \Phi' &= -\Phi_1 s_\beta + \Phi_2 c_\beta = \frac{1}{\sqrt{2}} \begin{pmatrix} \sqrt{2} H^+ \\ H' + iA \end{pmatrix}. \end{aligned} \quad (9)$$

⁵It is also called the Higgs basis; see Ref. [12] and references therein.

On the ray Eq. (5) on which V_0 has nontrivial extrema, these fields are

$$\Phi_\beta = \frac{1}{\sqrt{2}} \begin{pmatrix} 0 \\ \phi \end{pmatrix}, \quad \Phi'_\beta = \frac{1}{\sqrt{2}} \begin{pmatrix} 0 \\ 0 \end{pmatrix}, \quad (10)$$

The tree-level extremal conditions in this basis are

$$\left. \frac{\partial V_0}{\partial H} \right|_{\langle \rangle} = \phi^3 [\lambda_1 c_\beta^4 + \lambda_2 s_\beta^4 + \lambda_{345} s_\beta^2 c_\beta^2] = 0, \quad (11)$$

$$\left. \frac{\partial V_0}{\partial H'} \right|_{\langle \rangle} = \frac{1}{2} \phi^3 [(2\lambda_2 s_\beta^2 + \lambda_{345} c_\beta^2) - (2\lambda_1 c_\beta^2 + \lambda_{345} s_\beta^2)] s_\beta c_\beta = 0,$$

where $\langle \rangle$ means that the derivatives are evaluated at $\langle H \rangle = \phi$ while $\langle H' \rangle$ and all other VEVs equal zero. Using Eqs. (11), the tree potential is⁶

$$\begin{aligned} V_0 &= -2\lambda_{345} \left[\frac{1}{2} (\Phi^\dagger \Phi' + \Phi'^\dagger \Phi) + \Phi'^\dagger \Phi' \cot 2\beta \right]^2 \\ &\quad - \lambda_{45} [(\Phi^\dagger \Phi) (\Phi'^\dagger \Phi') - (\Phi^\dagger \Phi') (\Phi'^\dagger \Phi)] + \frac{1}{2} \lambda_5 [\Phi^\dagger \Phi' - \Phi'^\dagger \Phi]^2 \quad (12) \\ &= -\frac{1}{2} \lambda_{345} [HH' + zA + w^+ H^- + H^+ w^- + (H'^2 + A^2 + 2H^+ H^-) \cot 2\beta]^2 \\ &\quad - \frac{1}{2} \lambda_{45} [(H^2 + z^2) H^+ H^- + (H'^2 + A^2) w^+ w^- \\ &\quad \quad - (HH' + zA)(w^+ H^- + H^+ w^-) - i(HA - zH')(w^+ H^- - H^+ w^-)] \\ &\quad - \frac{1}{2} \lambda_5 [HA - zH' + i(w^+ H^- - H^+ w^-)]^2. \quad (13) \end{aligned}$$

The form of Eq. (13) will be used in Sec. II to define the mass-dependent scalar couplings that appear in the two-loop calculations. The tree-level “mass” matrices of the Higgs bosons are⁷

$$\mathcal{M}_{0^-}^2 = \begin{pmatrix} 0 & 0 \\ 0 & M_A^2 \end{pmatrix} \quad \text{with } M_A^2 = -\lambda_5 \phi^2; \quad (14)$$

$$\mathcal{M}_\pm^2 = \begin{pmatrix} 0 & 0 \\ 0 & M_{H^\pm}^2 \end{pmatrix} \quad \text{with } M_{H^\pm}^2 = -\frac{1}{2} \lambda_{45} \phi^2; \quad (15)$$

$$\mathcal{M}_{0^+}^2 = \begin{pmatrix} 0 & 0 \\ 0 & M_{H'}^2 \end{pmatrix} \quad \text{with } M_{H'}^2 = -\lambda_{345} \phi^2. \quad (16)$$

⁶Note that there are no higher powers of H, z, w^\pm than quadratic in Eq. (12).

⁷The quotes around “mass” are there because $0 < \phi < \infty$.

The Coleman-Weinberg effective potential in one-loop order is a sum over the heavy particles in the model [21, 13, 16]:

$$V_1 = \frac{1}{64\pi^2} \sum_n \alpha_n \overline{M}_n^4 \left(\ln \frac{\overline{M}_n^2}{\Lambda_{\text{GW}}^2} - k_n \right). \quad (17)$$

For $n = (W^\pm, Z, t_L + t_R^c, H', A, H^\pm)$, $\alpha_n = (6, 3, -12, 1, 1, 2)$ counts the degrees of freedom of particle n and $k_n = 5/6$ for the weak gauge bosons and $3/2$ for the scalars and the top-quark Weyl fermions.⁸ The background-field dependent masses \overline{M}_n^2 in Eq. (17) are [21, 16]

$$\overline{M}_n^2 = \begin{cases} M_n^2 (2 (\Phi^\dagger \Phi + \Phi'^\dagger \Phi') / \phi^2) = M_n^2 ((H^2 + H'^2 + \dots) / \phi^2), & n \neq t, b \\ M_t^2 (2 \Phi_1^\dagger \Phi_1 / (\phi c_\beta)^2) = M_t^2 ((H - H' \tan \beta)^2 + \dots) / (\phi)^2 & , \end{cases} \quad (18)$$

where $M_n^2 \propto \phi^2$ is the actual squared mass of particle n at scale ϕ . (We put $M_b^2 = 0$ in calculations.) The form of \overline{M}_t^2 is dictated by the type-I coupling of fermions to the Φ_1 doublet in Eq. (4).⁹ Finally, Λ_{GW} is a renormalization scale that will be fixed relative to the Higgs VEV $v = 246 \text{ GeV}$ in Eqs. (25–26) below.

Following GW [1], extremal conditions and masses are obtained by evaluating derivatives of the effective potential $V_{\text{eff}} = V_0 + V_1 + V_2 + \dots$ at $\langle \rangle$ + possible shifts δH and $\delta H'$ in the VEVs of H and H' .¹⁰ We assume that these shifts have a loop expansion, e.g., $\delta H' = \delta_1 H' + \delta_2 H' + \dots$. The extremal conditions at one-loop order are [1]

$$\left. \frac{\partial(V_0 + V_1)}{\partial H} \right|_{\langle \rangle + \delta_1 H + \delta_1 H'} = 0, \quad (19)$$

$$\left. \frac{\partial(V_0 + V_1)}{\partial H'} \right|_{\langle \rangle + \delta_1 H + \delta_1 H'} = 0. \quad (20)$$

⁸ V_1 is calculated in the Landau gauge using the $\overline{\text{MS}}$ renormalization scheme.

⁹To avoid the confusion of too much notation, we use the same symbol, e.g. H , for the quantum field of particle H and for its classical counterpart in the field-dependent masses. Context will dictate which field is being used. However, for clarity in the field-dependent cubic couplings introduced in Sec. IIb, we denote the classical counterpart of field H by H_c , etc.

¹⁰The VEVs of the mass eigenstate Higgs bosons, called H_1 and H_2 in Eq. (32), will be fixed to $\langle H_1 \rangle^2 + \langle H_2 \rangle^2 = v^2 = (246.2 \text{ GeV})^2$. Also see Eq. (47) and the accompanying footnote.

Expanding Eqs. (19,20) to $\mathcal{O}(V_1)$ and using Eq. (16), these conditions become

$$\left. \frac{\partial V_1}{\partial H} \right|_{\langle H \rangle = v} = \frac{1}{16\pi^2 v} \sum_n \alpha_n M_n^4 \left(\ln \frac{M_n^2}{\Lambda_{\text{GW}}^2} + \frac{1}{2} - k_n \right) = 0, \quad (21)$$

$$M_{H'}^2 \delta_1 H' - \frac{\alpha_t M_t^4 \tan \beta}{16\pi^2 v} \left(\ln \frac{M_t^2}{\Lambda_{\text{GW}}^2} + \frac{1}{2} - k_t \right) = 0, \quad (22)$$

where the derivative with respect to H' of the $n \neq t$ terms in V_1 vanishes because those terms are quadratic in H' . Thus,

$$\delta_1 H' = -\frac{1}{M_{H'}^2} \left. \frac{\partial V_1}{\partial H'} \right|_{\langle \rangle} = \frac{\alpha_t M_t^4 \tan \beta}{16\pi^2 M_{H'}^2 v} \left(\ln \frac{M_t^2}{\Lambda_{\text{GW}}^2} + \frac{1}{2} - k_t \right), \quad (23)$$

the typical tadpole result [22, 23]. Also, because $\delta_1 H$ is not determined in $\mathcal{O}(V_1)$, we are free to set it. We expect from Eq. (34) below that $\delta_1 H = \mathcal{O}(\delta_1 H' \times \delta_1) = \mathcal{O}(V_2)$, where δ_1 is the one-loop-induced H - H' mixing angle; therefore, we set

$$\delta_1 H = 0. \quad (24)$$

A particular scale $\phi = v$ appears in Eqs. (21, 22) because, for nontrivial extrema with $\beta \neq 0, \pi/2$, a deeper minimum than the *vanishing* zeroth-order ones *can* appear there: $(V_0 + V_1)|_{\langle H \rangle = v} < V_{0\beta} = V_0(0) + V_1(0) = 0$. In that case, Eq. (21) is equivalent to a relation between the renormalization scale Λ_{GW} and the Higgs VEV v :

$$\ln \left(\frac{\Lambda_{\text{GW}}^2}{v^2} \right) = \frac{A}{B} + \frac{1}{2}, \quad (25)$$

where

$$A = \sum_n \alpha_n M_n^4 \left(\ln \frac{M_n^2}{v^2} - k_n \right), \quad B = \sum_n \alpha_n M_n^4. \quad (26)$$

At $\langle \rangle$, $\overline{M}_n^2 = M_n^2$, and the effective potential is

$$(V_0 + V_1)|_{\langle \rangle} = \frac{1}{64\pi^2} \left(A + B \ln \frac{v^2}{\Lambda_{\text{GW}}^2} \right) = -\frac{B}{128\pi^2}. \quad (27)$$

Thus, unless $B > 0$, this extremum cannot be a minimum because otherwise it has no finite bottom for $v \rightarrow \infty$ [1]. Despite the large negative top-quark term in B , the contribution of the extra Higgs bosons can make it

positive. With the minimum occurring at the particular value $\phi = v$, the scale invariance of the tree approximation is now explicitly broken and the Higgs boson H gets a nonzero mass. Note that all $M_n^2 \propto v^2$ so that the right side of Eq. (25) is a function of only gauge, Higgs-boson and the top-quark Yukawa couplings. The VEVs of Φ_1 and Φ_2 are $v_1 = v \cos \beta$ and $v_2 = v \sin \beta$, with $\tan \beta = v_2/v_1$ as usual in a 2HDM.

The CP -even Higgs mass matrix to $\mathcal{O}(V_1)$ in the aligned basis is

$$\mathcal{M}_{0^+}^2 = \begin{pmatrix} (\partial^2 V_1 / \partial H^2) & (\partial^2 (V_0 + V_1) / \partial H \partial H') \\ (\partial^2 (V_0 + V_1) / \partial H \partial H') & (\partial^2 (V_0 + V_1) / \partial H'^2) \end{pmatrix}_{\langle \rangle + \delta_1 H'}, \quad (28)$$

where, again using Eq. (21),

$$\mathcal{M}_{HH}^2 = \left. \frac{\partial^2 V_1}{\partial H^2} \right|_{\langle \rangle} = \frac{1}{8\pi^2 v^2} \sum_n \alpha_n M_n^4 \equiv \frac{B}{8\pi^2 v^2}, \quad (29)$$

$$\begin{aligned} \mathcal{M}_{HH'}^2 &= \left. \frac{\partial^3 V_0}{\partial H \partial H'^2} \right|_{\langle \rangle} \delta_1 H' + \left. \frac{\partial^2 V_1}{\partial H \partial H'} \right|_{\langle \rangle} \\ &= \frac{2M_{H'}^2 \delta_1 H'}{v} - \frac{3\alpha_t M_t^4 \tan \beta}{16\pi^2 v^2} \left(\ln \frac{M_t^4}{\Lambda_{\text{GW}}^2} + \frac{7}{6} - k_t \right) \\ &= -\frac{\alpha_t M_t^4 \tan \beta}{16\pi^2 v^2} \left(\ln \frac{M_t^2}{\Lambda_{\text{GW}}^2} + \frac{5}{2} - k_t \right), \end{aligned} \quad (30)$$

$$\begin{aligned} \mathcal{M}_{H'H'}^2 &= \left. \frac{\partial^2 V_0}{\partial H'^2} \right|_{\langle \rangle} + \left. \frac{\partial^3 V_0}{\partial H'^3} \right|_{\langle \rangle} \delta_1 H' + \left. \frac{\partial^2 V_1}{\partial H'^2} \right|_{\langle \rangle} \\ &= M_{H'}^2 + \frac{6M_{H'}^2 \cot 2\beta \delta_1 H'}{v} \\ &\quad + \frac{\alpha_t M_t^4 (3 \tan^2 \beta - 1)}{16\pi^2 v^2} \left(\ln \frac{M_t^2}{\Lambda_{\text{GW}}^2} + \frac{1}{2} - k_t \right) + \frac{2\alpha_t M_t^4 \tan^2 \beta}{16\pi^2 v^2} \\ &= M_{H'}^2 + \frac{\alpha_t M_t^4}{8\pi^2 v^2} \left(\ln \frac{M_t^2}{\Lambda_{\text{GW}}^2} + \frac{1}{2} - k_t + \tan^2 \beta \right). \end{aligned} \quad (31)$$

The eigenvectors H_1 , H_2 and eigenvalues of $\mathcal{M}_{0^+}^2$, with $M_{H_1}^2 < M_{H_2}^2$, are

$$\begin{aligned} H_1 &= H \cos \delta_1 - H' \sin \delta_1, \\ H_2 &= H \sin \delta_1 + H' \cos \delta_1, \end{aligned} \quad (32)$$

$$\begin{aligned} M_{H_1}^2 &= \mathcal{M}_{HH}^2 \cos^2 \delta_1 + \mathcal{M}_{H'H'}^2 \sin^2 \delta_1 - 2\mathcal{M}_{HH'}^2 \sin \delta_1 \cos \delta_1, \\ M_{H_2}^2 &= \mathcal{M}_{HH}^2 \sin^2 \delta_1 + \mathcal{M}_{H'H'}^2 \cos^2 \delta_1 + 2\mathcal{M}_{HH'}^2 \sin \delta_1 \cos \delta_1, \end{aligned} \quad (33)$$

where δ_1 is the H - H' mixing angle δ in the *one-loop* approximation to

$$\tan 2\delta = \frac{2\mathcal{M}_{HH'}^2}{\mathcal{M}_{H'H'}^2 - \mathcal{M}_{HH}^2} \cong -\frac{\alpha_t M_t^4 \tan \beta}{8\pi^2 v^2 M_{H'}^2} \left(\ln \frac{M_t^2}{\Lambda_{\text{GW}}^2} + \frac{5}{2} - k_t \right) + \mathcal{O}(V_2). \quad (34)$$

These eigenmasses and the angle δ_1 are displayed for the GW-2HDM in Figs. 1, 2 and will be discussed below.

The one-loop GW-2HDM formula for the Higgs boson's mass, $M_H = 125$ GeV, is

$$M_H^2 = \frac{B}{8\pi^2 v^2} + \mathcal{O}(V_2) = \frac{1}{8\pi^2 v^2} (6M_W^4 + 3M_Z^4 + M_{H'}^4 + M_A^4 + 2M_{H^\pm}^4 - 12m_t^4). \quad (35)$$

Thus, B is positive, as required so that $(V_0 + V_1)|_{\langle \rangle} < 0$. This constrains the BSM Higgs masses and implies a simple and important sum rule on them:

$$(M_{H'}^4 + M_A^4 + 2M_{H^\pm}^4)^{1/4} = 540 \text{ GeV}. \quad (36)$$

This sum rule holds in the one-loop approximation of *any* GW model of electroweak symmetry breaking in which the only weak bosons are W and Z and the only heavy fermion is the top quark. Thus, the larger the Higgs sector, the lighter will be the masses of at least some of the BSM Higgs bosons expected in a GW model. Its importance is that these models predict extra Higgs bosons at surprisingly low masses. In the GW-2HDM, they have conventional decay modes, discussed at length in Refs. [8, 10, 11]. Determining the sum rule's reliability is a main motivation for extending the calculation of \mathcal{M}_{0+}^2 to two loops.

Equations (23) and (29)–(34) establish a connection between the top quark and Higgs alignment: If it were not for the Glashow-Weinberg constraint on the Higgs couplings to quarks [17] and the top quark's large mass (hence its appearance in V_1), $\delta_1 H'$ and δ_1 would vanish and \mathcal{M}_{0+}^2 would be diagonal [11]. This degree of Higgs alignment means that standard techniques of searching for the BSM Higgs bosons H' , A and H^\pm via their couplings to W^+W^- , ZZ and $W^\pm Z$, both in fusion production and decay and in $H', A \rightarrow ZH$ and $H^\pm \rightarrow HW^\pm$, will continue to come up empty-handed; see <https://twiki.cern.ch/twiki/bin/view/AtlasPublic> and <https://cms-results.web.cern.ch/cms-results/public-results/publications/>

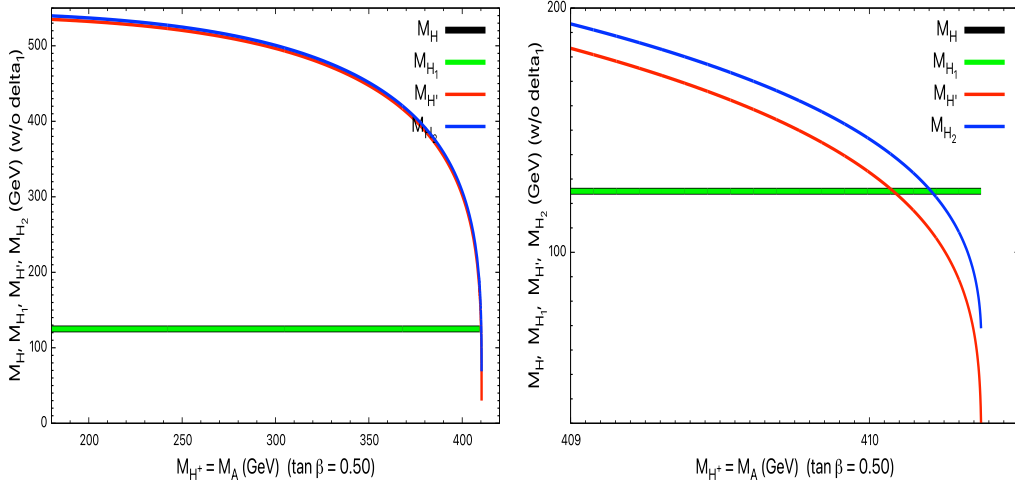


Figure 1: Left: The CP -even Higgs masses: $M_H = 125$ GeV in Eq. (35), $M_{H'}$ from the sum rule Eq. (36), and the eigenvalues M_{H_1} and M_{H_2} from Eq. (33) in the strict one-loop approximation. The masses are plotted vs. $M_A = M_{H^\pm}$ from 180 GeV to 410.5 GeV where $M_{H'}$ is rapidly approaching zero. Here, $\tan\beta = 0.50$ [8]; only small one-loop masses are sensitive to that choice. Right: A close-up of the endpoint of the tree-level and one-loop masses of the CP -even Higgs bosons.

HIG/SUS.html, and the electroweak couplings of the GW-2HDM scalars in Sec. IV, Eq. (68). The rates for these processes are proportional to $\delta_1^2 \sim (\delta_1 H'/v)^2 \lesssim 10^{-3}$ [8, 10]. An equivalent consequence of the top-quark's connection to alignment is that it is responsible for the one-loop VEV $\delta_1 H'$ acquired by the other CP -even Higgs, H' .

The nearly diagonal nature of \mathcal{M}_{0+}^2 — that $M_{H_1}^2 \equiv M_H^2 \cong M_{HH}^2$ and $M_{H_2}^2 \cong M_{H'H'}^2$ — is illustrated in Fig. 1 where the mass pairs are plotted versus $M_A = M_{H^\pm}$. In the left panel, where $180 \text{ GeV} \leq M_{H^\pm, A} < 410.5 \text{ GeV}$, the masses in each pair appear to be on top of other each other. As the sum rule (36) forces $M_{H'} \rightarrow 0$ at $M_A = M_{H^\pm} = 410.5 \text{ GeV}$, the difference in the H' mass pairs due to the top-quark term in $\mathcal{M}_{H'H'}^2$ is seen in the right panel.

Examples of how unimportant the top-quark terms are, except for small

$M_{H'}$, are displayed in Table 1. Note how sensitive $M_{H'}$ and the eigenvalues M_{H_2} are as the endpoint of the sum rule (36) is approached.

$M_A = M_{H^\pm}$	$M_{H'}$	δ_1	$\delta_1 H'$	M_{H_2}
375.0	400.6	0.76×10^{-3}	1.55	404.9
409.8	147.6	0.31×10^{-2}	12.3	160.0
410.21	108.7	0.603×10^{-1}	22.9	125.2

Table 1: Examples of the approach to the breakdown of the validity of the one-loop expansion as the endpoint $M_A = 410.5$ GeV of the sum rule (36) is approached. Masses are in GeV and $\tan \beta = 0.50$.

Reference [16] demonstrated a level repulsion between M_{H_1} and M_{H_2} as $M_{H'} \rightarrow 0$. We can reproduce that here by using the full Eq (33) with $\tan \delta_1$ given by using all $\mathcal{O}(V_1)$ terms in the first equality of Eq. (34). This gives contributions of $\mathcal{O}(V_2)$ which become appreciable to the eigenmasses when $M_{H'} \rightarrow 0$. We illustrate this in Fig. 2. In the left panel the angle $|\delta_1|$ is plotted vs. M_A . Below $M_A \simeq 380$ GeV the angle is very small, $|\delta_1| \lesssim 10^{-3}$ and it changed sign from negative to positive at $M_A = 315$ GeV. Above $M_A \simeq 380$ GeV, the sum rule starts to force $M_{H'} \rightarrow 0$, the denominator $\mathcal{M}_{H'H'}^2 - \mathcal{M}_{HH}^2$ in $\tan \delta_1$ decreases rapidly above $M_{H^\pm, A} = 410$ GeV, changing sign at 410.14 GeV. Consequently, $|\delta_1|$ rises rapidly from $\sim 10^{-3}$, passing through $\pi/4$ on its way to $\pi/2$ when $M_{H'} \rightarrow 0$. Here, this excursion of the mixing angle is the signal of level repulsion, clearly seen in the right panel. The magnitude of the angle δ_1 and the swapping of the two CP -even levels in this region signal the breakdown of the validity of the loop perturbation expansion.¹¹

In Sec. IIa we present a formalism for calculating the extremal conditions and the CP -even masses of the two-loop effective potential, $V_{\text{eff}} = V_0 + V_1 + V_2$, of the GW-2HDM model. This formalism is the straightforward generalization to two loops of that in Ref. [1]. Still working in the aligned basis, we expand derivatives of V_{eff} about their zeroth-order VEVs (Eq. (10))

¹¹The explanation for this phenomenon in Ref. [8] was incorrect also, but for a different reason.

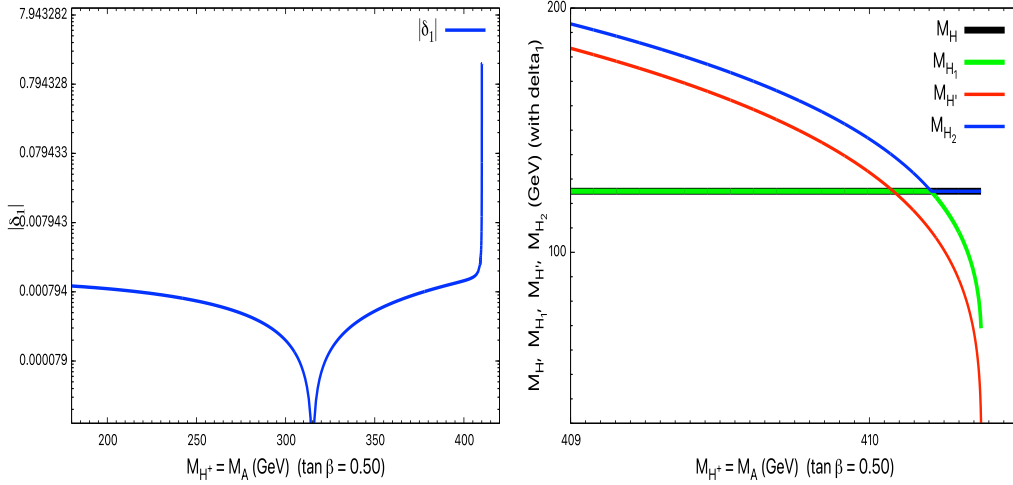


Figure 2: The magnitude of the one-loop $H-H'$ mixing angle δ_1 (in radians) vs. $M_A = M_{H^\pm}$ at $\tan \beta = 0.50$. Note that $\mathcal{M}_{HH'}^2$, $\delta_1 \propto \tan \beta$. Left: The full range from $M_{H^\pm, A} = 180$ GeV to the sum rule cutoff at 410.5 GeV. Below $M_{H^\pm, A} = 315$ GeV the numerator $\mathcal{M}_{HH'}^2$ of $\tan 2\delta_1$ is negative and so is δ_1 ; $\mathcal{M}_{HH'}^2$ and δ_1 change sign at $M_{H^\pm, A} = 315$ GeV. Right: A close-up of masses at the endpoint as $M_{H'} \rightarrow 0$, showing the level repulsion at $M_A = 410.2$ GeV between M_{H_1} and M_{H_2} . There, $M_{H_1} \rightarrow M_{H'}$ and $M_{H_2} \rightarrow M_H = 125$ GeV. In this region $\delta_1 \geq \pi/4$ and the validity of the loop perturbation expansion has broken down.

allowing for shifts in the VEV's of H and H' while keeping their RMS equal to v (see Eq. (47)). In these calculations, we keep terms of at most $\mathcal{O}(V_2)$, discarding those that are formally of higher order in the loop expansion. We call this procedure the ‘‘perturbative method.’’

In Sec. IIb we simplify our calculation considerably by keeping only the all-Higgs-scalar terms in V_2 . This is quite a good approximation for this method; see Fig. 3. In this section we follow Martin [13] and define the field-dependent triple-scalar couplings needed for these calculations.

Even in this approximation, the two-loop generalization of Eqs. (35, 36) is intractable, so we must resort to a purely numerical scheme to determine

the BSM scalar masses in terms of M_{H_1} and M_W, M_Z, M_t . This is done in Secs. IIb,c. The basis of this scheme is that, to $\mathcal{O}(V_2)$, the CP -even mass-squared matrix \mathcal{M}_{0+}^2 has positive eigenvalues with $M_{H_1}^2$ close to $(125 \text{ GeV})^2$. For this, the two-loop extremal conditions are used to determine the corrections to Λ_{GW} and the shifts $\delta_2 H, \delta_2 H'$ in the CP -even Higgs VEVs. This procedure does not guarantee that $\det(\mathcal{M}_{0+}^2) > 0$ for the allowed range of $M_A = M_{H^\pm}$ and $M_{H'}$ as it does in $\mathcal{O}(V_1)$. This determinant has terms of $\mathcal{O}(V_4)$, coming from the square of $\mathcal{M}_{HH'}^2$, for example, and they are not small. But it does not contain all fourth-order terms; others will come from the three- and four-loop effective potential.¹²

We find two “branches”, $B1$ and $B2$, of the H_2 mass for $M_{H_1} \cong 125 \text{ GeV}$ and $M_A = M_{H^\pm} \geq 180 \text{ GeV}$. In the lower-mass branch, $B1$, the plot of M_{H_2} vs. $M_A = M_{H^\pm}$ is reminiscent of the left panel in Fig. 1. This behavior is not the result of a simple sum rule like Eq. (36), but the cause is much the same: requiring $M_{H_1} = 125 \text{ GeV}$ restricts M_{H_2} to small values for large $M_A = M_{H^\pm}$. In this branch, which extends over $180 \leq M_A = M_{H^\pm} \lesssim 380 \text{ GeV}$, M_{H_2} starts near 550 GeV , rises to 700 GeV and then drops rapidly to near zero at $M_A^* \cong 380 \text{ GeV}$. From there, branch $B2$ rises rapidly and grows together indefinitely with the increasing input $M_{H'}$. For reasons we discuss in Sec. IIc, we consider only branch $B1$ to be physically meaningful.

As in perturbation theory in ordinary quantum mechanics, determining the mass eigenvalues to $\mathcal{O}(V_2)$ requires that we know the eigenvectors H_1 and H_2 only to $\mathcal{O}(V_1)$. To that extent, what we have already stated about the degree of Higgs alignment — that H_1 very nearly has SM couplings and that such processes as $H', A \rightarrow W^+W^-, ZZ$ and HZ are greatly suppressed — is still correct. Furthermore, alignment remains strong if we use the $\mathcal{O}(V_1)$ approximation to just the numerator of Eq. (34) for $\tan 2\delta$ (see Eq. (53)).

In Sec. III we follow a different approach to calculating the eigenvalues of \mathcal{M}_{0+}^2 . It requires that the full two-loop effective potential, $V_0 + V_1 + V_2$, has a stable minimum. The program *Amoeba* [24] is used to find the regions of V_{eff} for which \mathcal{M}_{0+}^2 is positive-definite. We vary $M_A = M_{H^\pm}$ and $M_{H'}$ and require that M_{H_1} or M_{H_2} is equal 125 GeV . Only the solutions with the

¹²This seems to be a problem with no end unless successive loop contributions become negligibly small. Another facet of this will occur in Sec. III.

lighter eigenmass $M_{H_1} = 125 \text{ GeV}$ are consistent with LEP and LHC Higgs boson searches. We call this procedure the “amoeba method”. As in Sec. IIc, there are two regions of $M_A = M_{H^\pm}$ for this solution that we also call $B1$ and $B2$. Region $B1$ extends from $M_A \cong 290 \text{ GeV}$ to 425 GeV and $B2$ from 425 GeV to about 600 GeV . Again, only region $B1$ is physically meaningful. The behavior of the eigenvalue M_{H_2} is quite similar in the $B1$ region of both methods as are the transitions between regions $B1$ and $B2$.

Finally, in Sec. IV we discuss the experimental implications of our two-loop studies, especially as they refer to the LHC experiments ATLAS and CMS. They are in good agreement with those in our previous papers [8],[10],[11]: The BSM Higgs bosons are well within reach of the LHC today, but their discovery requires much improvement in the rejection of low-energy QCD backgrounds. We discuss two new search modes that have low rates, but also much lower backgrounds. Higgs alignment is respected with experimental violations and the corresponding suppression of many processes enjoyed by the SM Higgs below $\mathcal{O}(1\%)$.

II. The GW-2HDM at two-loops: the perturbative method

Gildener and Weinberg’s one-loop analysis [1] started from Eqs. (19,20). Because their analysis was intentionally model-independent, its main result was the very general, and very important, Eq. (29) for the Higgs boson’s mass. In the specific GW-2HDM, we can do more and extract other results. The most important ones so far are the sum rule (36) constraining the masses of the model’s BSM Higgs bosons to be light and the degree to which Higgs alignment and the related suppression of BSM couplings to weak boson pairs and to a weak boson plus the SM Higgs H . Determining the degrees to which they hold when extended to two loops motivate our present investigation.

We divide the discussion in this section into three parts: (a) The formalism for the extremal conditions and the two-loop contributions to the CP -even scalar masses. This includes the generalization to two-loop order of Eq. (25) relating the renormalization scale Λ_{GW} to the electroweak VEV v .

(b) Calculations of Λ_{GW} and \mathcal{M}_{0+}^2 in the approximation of keeping *only* the all-scalar terms in V_2 . (c) Determining the allowed ranges of the BSM masses, $M_A = M_{H^\pm}$ and M_{H_2} for $M_{H_1} = 125 \text{ GeV}$, and the degree of Higgs alignment in the GW-2HDM. We refer to this procedure as the ‘‘perturbative method’’ because we discard terms that are formally of higher order than two loops.

IIa. The two-loop formalism

We extend the analysis in Ref. [1] to two-loop order here. The key requirement of this is to retain only those terms that are at most formally of second order in the loop expansion. The aligned basis, Eq. (9), is still the most suitable for this because, as we shall see, the strictly two-loop corrections to Higgs alignment are small. In the CP -conserving GW-2HDM, the only fields that can acquire a VEV are the CP -even H and H' . Therefore, through $\mathcal{O}(V_2)$, and using $\delta_1 H = 0$, the extremal conditions are obtained from

$$\left. \frac{\partial(V_0 + V_1 + V_2)}{\partial H} \right|_{\langle \rangle + \delta_1 H' + \delta_2 H' + \delta_2 H} = 0, \quad (37)$$

$$\left. \frac{\partial(V_0 + V_1 + V_2)}{\partial H'} \right|_{\langle \rangle + \delta_1 H' + \delta_2 H' + \delta_2 H} = 0, \quad (38)$$

where, again, $\langle \rangle$ means the tree-level VEVs $\langle H \rangle = v$ and $\langle H' \rangle = 0$. Using the vanishing derivatives of V_0 in Eqs. (11,16) and $(\partial^3 V_0 / \partial H^3)_{\langle \rangle} = (\partial^4 V_0 / \partial H^4)_{\langle \rangle} = 0$, we get:

$$\begin{aligned} 0 &= \left. \frac{\partial(V_0 + V_1 + V_2)}{\partial H} \right|_{\langle \rangle + \delta_1 H' + \delta_2 H' + \delta_2 H} \\ &= \left. \frac{\partial V_1}{\partial H} \right|_{\langle \rangle} + \frac{1}{2} \left. \frac{\partial^3 V_0}{\partial H \partial H'^2} \right|_{\langle \rangle} (\delta_1 H')^2 + \left. \frac{\partial^2 V_1}{\partial H \partial H'} \right|_{\langle \rangle} \delta_1 H' + \left. \frac{\partial V_2}{\partial H} \right|_{\langle \rangle} \\ &= \frac{1}{16\pi^2 v} \sum_n \alpha_n M_n^4 \left(\ln \frac{M_n^2}{\Lambda_{\text{GW}}^2} + \frac{1}{2} - k_n \right) \\ &\quad - \frac{\alpha_t M_t^4 \tan \beta \delta_1 H'}{8\pi^2 v^2} \left(\ln \frac{M_t^2}{\Lambda_{\text{GW}}^2} + \frac{3}{2} - k_t \right) + \left. \frac{\partial V_2}{\partial H} \right|_{\langle \rangle}; \end{aligned} \quad (39)$$

$$\begin{aligned}
0 &= \left. \frac{\partial(V_0 + V_1 + V_2)}{\partial H'} \right|_{\langle \rangle + \delta_1 H' + \delta_2 H' + \delta_2 H} \\
&= \left. \frac{\partial^2 V_0}{\partial H'^2} \right|_{\langle \rangle} \delta_1 H' + \left. \frac{\partial V_1}{\partial H'} \right|_{\langle \rangle} + \left. \frac{\partial^2 V_0}{\partial H'^2} \right|_{\langle \rangle} \delta_2 H' + \left. \frac{\partial^2 V_1}{\partial H'^2} \right|_{\langle \rangle} \delta_1 H' + \frac{1}{2} \left. \frac{\partial^3 V_0}{\partial H'^3} \right|_{\langle \rangle} (\delta_1 H')^2 + \left. \frac{\partial V_2}{\partial H'} \right|_{\langle \rangle} \\
&= \left[\frac{\alpha_t M_t^4 (1 + 3 \tan^2 \beta)}{32 \pi^2 v^2} \left(\ln \frac{M_t^2}{\Lambda_{\text{GW}}^2} + \frac{1}{2} - k_t \right) + \frac{\alpha_t M_t^4 \tan^2 \beta}{8 \pi^2 v^2} \right. \\
&\quad \left. + \frac{1}{16 \pi^2 v} \sum_n \alpha_n M_n^4 \left(\ln \frac{M_n^2}{\Lambda_{\text{GW}}^2} + \frac{1}{2} - k_n \right) \right] \delta_1 H' + M_{H'}^2 \delta_2 H' + \left. \frac{\partial V_2}{\partial H'} \right|_{\langle \rangle}. \tag{40}
\end{aligned}$$

Here, we used Eq. (13) to calculate the derivatives of V_0 , the definition of the $\mathcal{O}(V_1)$ shift $\delta_1 H'$ in the VEV of H' , in Eq. (22), and the following:

$$\left. \frac{\partial V_1}{\partial H} \right|_{\langle \rangle} = \frac{1}{16 \pi^2 v} \sum_n \alpha_n M_n^4 \left(\ln \frac{M_n^2}{\Lambda_{\text{GW}}^2} + \frac{1}{2} - k_n \right) \tag{41}$$

$$\left. \frac{\partial^2 V_1}{\partial H \partial H'} \right|_{\langle \rangle} = -\frac{3 \alpha_t M_t^4 \tan \beta}{16 \pi^2 v^2} \left(\ln \frac{M_t^2}{\Lambda_{\text{GW}}^2} + \frac{7}{6} - k_t \right), \tag{42}$$

$$\begin{aligned}
\left. \frac{\partial^2 V_1}{\partial H'^2} \right|_{\langle \rangle} &= \frac{\alpha_t M_t^4 (3 \tan^2 \beta - 1)}{16 \pi^2 v^2} \left(\ln \frac{M_t^2}{\Lambda_{\text{GW}}^2} + \frac{1}{2} - k_t \right) + \frac{2 \alpha_t M_t^4 \tan^2 \beta}{16 \pi^2 v^2} \\
&\quad + \frac{1}{16 \pi^2 v^2} \sum_n \alpha_n M_n^4 \left(\ln \frac{M_n^2}{\Lambda_{\text{GW}}^2} + \frac{1}{2} - k_n \right). \tag{43}
\end{aligned}$$

Every term on the right side of Eqs. (39,40) is of $\mathcal{O}(V_2)$ or, sometimes more explicitly, $\mathcal{O}(\kappa^2)$, where

$$\kappa = \frac{1}{16 \pi^2}. \tag{44}$$

This is because, as stated below Eq. (7), the extremal conditions in each order of the loop expansion of V_{eff} are enforced in all orders of the loop expansion [1]. That means, e.g., that the right side of Eq. (41 and the third term in Eq. (43) are $\mathcal{O}(V_2)$. This will provide an $\mathcal{O}(V_2)$ correction to Λ_{GW} .

The dominant $\mathcal{O}(\kappa^2)$ corrections to the extremal conditions will come from the derivatives of V_2 itself with respect to H and H' . Equation (39) determines the $\mathcal{O}(V_1) = \mathcal{O}(\kappa)$ correction to Λ_{GW} . From now on, we denote the renormalization scale by Λ_{GW} *only* in terms that are otherwise of $\mathcal{O}(V_1)$. In those terms, the $\mathcal{O}(V_1)$ part of Λ_{GW} will produce an $\mathcal{O}(\kappa^2)$ contribution. In

terms that are already $\mathcal{O}(V_2)$, we use the $\mathcal{O}(\kappa^0)$ scale $\Lambda_0 = v \exp(\frac{1}{2}(A/B + \frac{1}{2}))$ from Eq. (25). We obtain the following expression for Λ_{GW} (in which we still use $M_H^2 = (\partial^2 V_1 / \partial H^2)_{\langle \rangle} = \sum_n \alpha_n M_n^4 / 8\pi^2 v^2$):

$$\begin{aligned} \Lambda_{\text{GW}} &= \Lambda_0 \exp \left\{ \frac{2}{M_H^2 v} \left[\frac{\alpha_t M_t^4 \tan \beta \delta_1 H'}{8\pi^2 v^2} \left(\log \frac{M_t^2}{\Lambda_0^2} + \frac{3}{2} - k_t \right) - \frac{\partial V_2}{\partial H} \Big|_{\langle \rangle} \right] \right\} \\ &\cong \Lambda_0 \left[1 + \frac{\alpha_t M_t^4 \tan \beta \delta_1 H'}{4\pi^2 v^3 M_H^2} \left(\log \frac{M_t^2}{\Lambda_0^2} + \frac{3}{2} - k_t \right) - \frac{2}{M_H^2 v} \frac{\partial V_2}{\partial H} \Big|_{\langle \rangle} \right]. \end{aligned} \quad (45)$$

This correction to Λ_0 is $\mathcal{O}(\kappa)$ because $M_H^2 = \mathcal{O}(\kappa)$.

Equation (40) determines the $\mathcal{O}(\kappa^2)$ contribution $\delta_2 H'$ to $\delta H'$:

$$\begin{aligned} \delta_2 H' &= -\frac{1}{M_{H'}^2} \left[\frac{1}{2} \frac{\partial^3 V_0}{\partial H'^3} \Big|_{\langle \rangle} (\delta_1 H')^2 + \frac{\partial^2 V_1}{\partial H'^2} \Big|_{\langle \rangle} \delta_1 H' + \frac{\partial V_2}{\partial H'} \Big|_{\langle \rangle} \right] \\ &= -\frac{1}{M_{H'}^2} \left[\left(\frac{\alpha_t M_t^4 (1 + 3 \tan^2 \beta)}{32\pi^2 v^2} \left(\ln \frac{M_t^2}{\Lambda_0^2} + \frac{1}{2} - k_t \right) + \frac{\alpha_t M_t^4 \tan^2 \beta}{8\pi^2 v^2} \right) \delta_1 H' + \frac{\partial V_2}{\partial H'} \Big|_{\langle \rangle} \right]. \end{aligned} \quad (46)$$

The shift $\delta_2 H$ does not appear in Eqs. (39,40). It could do so to $\mathcal{O}(V_2)$ only by multiplying $(\partial^2 V_0 / \partial H^2)_{\langle \rangle} = 0$ and $(\partial^2 V_0 / \partial H \partial H')_{\langle \rangle} = 0$ by $\delta_2 H$. Since it is undetermined, we use it to keep v fixed. That is, we require¹³

$$v^2 = (v + \delta_2 H)^2 + (\delta_1 H' + \delta_2 H')^2 \implies \delta_2 H = -(\delta_1 H')^2 / 2v. \quad (47)$$

Now turn to the elements of the CP -even squared mass matrix in $\mathcal{O}(V_2)$. With an obvious notation, they are:

$$\begin{aligned} \left(\mathcal{M}_{H_i H_j}^2 \right)_2 &= \frac{\partial^2 (V_0 + V_1 + V_2)}{\partial H_i \partial H_j} \Big|_{\langle \rangle + \delta H + \delta H'} \\ &= \frac{\partial^2 V_0}{\partial H_i \partial H_j} \Big|_{\langle \rangle} + \frac{\partial^3 V_0}{\partial H_i \partial H_j \partial H_k} \Big|_{\langle \rangle} (\delta_1 H_k + \delta_2 H_k) + \frac{1}{2} \frac{\partial^4 V_0}{\partial H_i \partial H_j \partial H_k \partial H_l} \Big|_{\langle \rangle} \delta_1 H_k \delta_1 H_l \\ &\quad + \frac{\partial^2 V_1}{\partial H_i \partial H_j} \Big|_{\langle \rangle} + \frac{\partial^3 V_1}{\partial H_i \partial H_j \partial H_k} \Big|_{\langle \rangle} \delta_1 H_k + \frac{\partial^2 V_2}{\partial H_i \partial H_j} \Big|_{\langle \rangle}. \end{aligned} \quad (48)$$

¹³Eq. (47) is correct through $\mathcal{O}(V_2)$.

Then:

$$\begin{aligned}
(\mathcal{M}_{HH}^2)_2 &= M_H^2 + M_{H'}^2 \left(\frac{\delta_1 H'}{v} \right)^2 - \frac{3\alpha_t M_t^4 \tan \beta}{8\pi^2 v^2} \left(\ln \frac{M_t^2}{\Lambda_0^2} + \frac{13}{6} - k_t \right) \frac{\delta_1 H'}{v} + \frac{\partial^2 V_2}{\partial H^2} \Big|_{\langle \rangle} \\
&= M_H^2 - \frac{5\alpha_t M_t^4 \tan \beta}{16\pi^2 v^2} \left(\ln \frac{M_t^2}{\Lambda_0^2} + \frac{5}{2} - k_t \right) \frac{\delta_1 H'}{v} + \frac{\partial^2 V_2}{\partial H^2} \Big|_{\langle \rangle}; \tag{49}
\end{aligned}$$

$$\begin{aligned}
(\mathcal{M}_{HH'}^2)_2 &= -\frac{\alpha_t M_t^4 \tan \beta}{16\pi^2 v^2} \left(\ln \frac{M_t^2}{\Lambda_{\text{GW}}^2} + \frac{5}{2} - k_t \right) \\
&+ \left[M_H^2 + \frac{3\alpha_t M_t^4 (\tan^2 \beta - 1)}{32\pi^2 v^2} \left(\ln \frac{M_t^2}{\Lambda_0^2} + \frac{1}{2} - k_t \right) + \frac{\alpha_t M_t^4 (3 \tan^2 \beta - 1)}{8\pi^2 v^2} \right] \frac{\delta_1 H'}{v} \\
&- \frac{2}{v} \frac{\partial V_2}{\partial H'} \Big|_{\langle \rangle} + \frac{\partial^2 V_2}{\partial H \partial H'} \Big|_{\langle \rangle}; \tag{50}
\end{aligned}$$

$$\begin{aligned}
(\mathcal{M}_{H'H'}^2)_2 &= M_{H'}^2 + \frac{\alpha_t M_t^4}{8\pi^2 v^2} \left(\ln \frac{M_t^2}{\Lambda_{\text{GW}}^2} + \frac{1}{2} - k_t + \tan^2 \beta \right) \\
&- \left[\frac{7\alpha_t M_t^4 \tan \beta}{16\pi^2 v^2} \left(\ln \frac{M_t^2}{\Lambda_0^2} + \frac{1}{2} - k_t \right) + \frac{\alpha_t M_t^4 \tan \beta (3 + 2 \tan^2 \beta)}{8\pi^2 v^2} \right] \frac{\delta_1 H'}{v} \\
&- \frac{6 \cot 2\beta}{v} \frac{\partial V_2}{\partial H'} \Big|_{\langle \rangle} + \frac{\partial^2 V_2}{\partial H'^2} \Big|_{\langle \rangle}. \tag{51}
\end{aligned}$$

Equation (47) for $\delta_2 H$ was used in calculating $\mathcal{M}_{H'H'}^2$.

When determining the eigenmasses M_{H_1, H_2}^2 in Eqs. (33) to $\mathcal{O}(V_2)$, *only* the $\mathcal{O}(\kappa)$ term in $\mathcal{M}_{HH'}^2$ should be kept (using Λ_0) and then multiplied by $\sin \delta_1 \cos \delta_1 = \mathcal{O}(\kappa)$. For the same reason, the term $\sin^2 \delta_1 \mathcal{M}_{HH}^2$ in $M_{H_2}^2$ should be dropped. The eigenvalues of \mathcal{M}_{0+}^2 to $\mathcal{O}(V_2)$ are then

$$\begin{aligned}
M_{H_1}^2 &= (\mathcal{M}_{HH}^2)_2 \cos^2 \delta_1 + (\mathcal{M}_{H'H'}^2)_0 \sin^2 \delta_1 - 2 (\mathcal{M}_{HH'}^2)_1 \sin \delta_1 \cos \delta_1, \\
M_{H_2}^2 &= (\mathcal{M}_{H'H'}^2)_2 \cos^2 \delta_1 + 2 (\mathcal{M}_{HH'}^2)_1 \sin \delta_1 \cos \delta_1, \tag{52}
\end{aligned}$$

where only the $\mathcal{O}(V_1)$ part of $\tan 2\delta_1 \cong 2\mathcal{M}_{HH'}^2 / \mathcal{M}_{H'H'}^2$ in Eq. (34) is used. The left side of Fig. 1 shows that these are good approximations.

On the other hand, for the purpose of determining the eigenvectors H_1 and H_2 and their degree of alignment from the $\mathcal{O}(V_2)$ version of Eq. (32), we use δ_2 defined by

$$\tan 2\delta_2 = \frac{(2\mathcal{M}_{HH'}^2)_1}{(\mathcal{M}_{H'H'}^2 - \mathcal{M}_{HH}^2)_2} \tag{53}$$

because this approximation is numerically closer to δ_1 than that which results from expanding $\tan 2\delta$ to $\mathcal{O}(\kappa^2)$.

I Ib. The scalar approximation

There are five general types of contributions to the two-loop potential V_2 for the GW-2HDM and similar electroweak models; see Secs. 2 and 4 of Ref. [13] for details of the interactions and the two-loop integrals.

- 1.) Scalar graphs consisting of “cracked-egg” two-vertex graphs with three scalars emanating from one interaction vertex and propagating to the other (SSS), and “figure-eight” graphs with two separate one-loop graphs (each loop as in V_1) stuck together at a single vertex with the appropriate quartic coupling (SS). These contributions arise from the scalar potential V_0 in Eq. (13), as described below.
- 2.) Cracked-egg fermion loops, induced by Yukawa interactions, with a scalar exchanged between the two vertices (FFS); only the top and bottom quarks contribute significantly to the loop integrals.
- 3.) From the electroweak gauge interactions of the scalars there are cracked-egg scalar loops with an electroweak gauge boson exchanged between the two vertices (SSV) and figure-eight graphs with a scalar loop and a gauge loop (VS). There are also cracked-egg electroweak gauge loops with a scalar exchanged between the vertices (VVS).
- 4.) Cracked-egg fermion loops with an electroweak boson or QCD gluon exchanged between the two vertices (FFV); again, only t and b quarks contribute substantially.
- 5.) Pure gauge-boson (including ghosts) cracked-egg and figure-eight loops (gauge).

Of these five types of contributions to V_2 , the scalar (SSS and SS) graphs are by far the most important because the BSM Higgs masses set their mag-

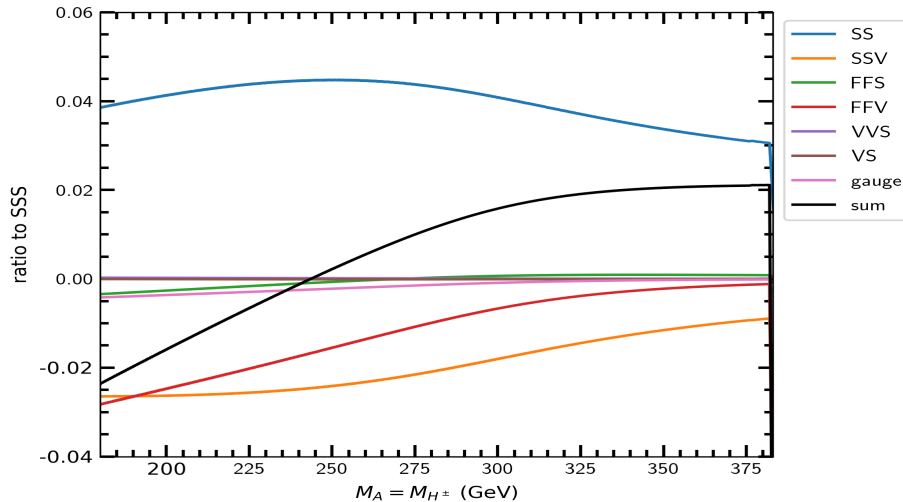


Figure 3: Ratios to the SSS cracked-egg contribution of the SS figure-eight, SSV, FFS, FFV, VVS, VS figure-eight, and gauge contributions to V_2 for $180 \text{ GeV} \leq M_A = M_{H^\pm} \lesssim 380 \text{ GeV}$, the region of branch $B1$ in Fig. 5. The black curve is the sum of the eight ratios. In addition to V_{SSS} and V_{SS} , these two-loop potentials are taken from Martin [13].

nitudes.^{14,15} Therefore, we approximate V_2 by its scalar contributions. This approximation is good to about 2% over the entire range of branch $B1$; see Fig. 3.

The SSS couplings descend from the quartic couplings in V_0 of Eq. (13) by shifting the scalar quantum fields by their classical counterparts [21].¹⁶ Following Ref. [13], it is convenient to use real scalar (and electroweak boson)

¹⁴As in V_1 , the tree-level masses are used for all the scalars, gauge bosons and fermions propagating in these loops.

¹⁵The cracked-egg scalar graphs are much larger than the figure eights; see also Ref. [25].

¹⁶The only other cracked-egg graphs with field-dependent couplings are VVS with V an electroweak boson. They descend from the quartic electroweak interactions and are of order a squared electroweak coupling times H_c or H'_c .

fields for this discussion:

$$\begin{aligned}
R_1 &= H', \quad R_2 = A, \quad R_3 = h_1, \quad R_4 = h_2; \\
R_5 &= H, \quad R_6 = z, \quad R_7 = w_1, \quad R_8 = w_2. \\
A_\mu^1 &= W_\mu^1, \quad A_\mu^2 = W_\mu^2, \quad A_\mu^3 = Z_\mu, \quad A_\mu^4 = A_\mu \text{ (the photon)}.
\end{aligned} \tag{54}$$

Here, $H^\pm = (h_1 \pm ih_2)/\sqrt{2}$, $w^\pm = (w_1 \pm iw_2)/\sqrt{2}$ and $W_\mu^\pm = (A_\mu^1 \pm iA_\mu^2)/\sqrt{2}$. Because our interest in calculating V_2 is to see its effect on M_{H_2} as we vary $M_A = M_{H^\pm}$ (as the sum rule (36) did in $\mathcal{O}(V_1)$) and on the H - H' mixing determining the departure from Higgs alignment, we shift only the two scalar fields that can get a CP -conserving VEV, H and H' :¹⁷

$$R_5 = H \rightarrow R_5 + H_c, \quad R_1 = H' \rightarrow R_1 + H'_c. \tag{55}$$

The cubic-scalar interactions are those that are first order in H_c or H'_c .¹⁸ We indicate these couplings with an *overbar*, $\bar{\lambda}_{ijk}$, as we did for the field-dependent masses \bar{M}_n^2 in Eq. (18).

The scalar interactions used in constructing V_2 of the GW-2HDM are then

$$V_S = \frac{1}{6} \bar{\lambda}_{ijk} R_i R_j R_k + \frac{1}{24} \lambda_{ijkl} R_i R_j R_k R_l, \tag{56}$$

where repeated indices are summed over and the prefactors of $\frac{1}{6}$ and $\frac{1}{24}$ are choices of convenience made in Ref. [13]. The triple-scalar couplings

¹⁷Strictly speaking, the derivatives with respect to H and H' in Secs. I and IIa were with respect to H_c and H'_c , but the results there do not depend on this point; also see footnote 9.

¹⁸The terms quadratic in the classical fields gave rise to the one-loop potential V_1 [21].

consistent with these normalizations are:

$$\begin{aligned}
\bar{\lambda}_{111} &= 6M_{H'}^2 \cot 2\beta (H_c + 2H'_c \cot 2\beta)/v^2; \\
\bar{\lambda}_{122} &= \bar{\lambda}_{133} = \bar{\lambda}_{144} = 2M_{H'}^2 \cot 2\beta (H_c + 2H'_c \cot 2\beta)/v^2; \\
\bar{\lambda}_{115} &= 2M_{H'}^2 (H_c + 3H'_c \cot 2\beta)/v^2, \quad \bar{\lambda}_{225} = 2(M_{H'}^2 H'_c \cot 2\beta + M_A^2 H_c)/v^2; \\
\bar{\lambda}_{335} &= \bar{\lambda}_{445} = 2(M_{H'}^2 H'_c \cot 2\beta + M_{H^\pm}^2 H_c)/v^2; \\
\bar{\lambda}_{155} &= 2M_{H'}^2 H'_c/v^2, \quad \bar{\lambda}_{166} = 2M_A^2 H'_c/v^2, \quad \bar{\lambda}_{177} = \bar{\lambda}_{188} = 2M_{H^\pm}^2 H'_c/v^2; \\
\bar{\lambda}_{126} &= (M_{H'}^2 - M_A^2)H_c/v^2, \quad \bar{\lambda}_{256} = (M_{H'}^2 - M_A^2)H'_c/v^2; \\
\bar{\lambda}_{137} &= \bar{\lambda}_{148} = ((M_{H'}^2 - M_{H^\pm}^2)H_c + 2M_{H'}^2 H'_c \cot 2\beta)/v^2; \\
\bar{\lambda}_{357} &= \bar{\lambda}_{458} = (M_{H'}^2 - M_{H^\pm}^2)H'_c/v^2; \\
\bar{\lambda}_{238} &= -\bar{\lambda}_{247} = (M_A^2 - M_{H^\pm}^2)H_c/v^2, \quad \bar{\lambda}_{467} = -\bar{\lambda}_{368} = (M_A^2 - M_{H^\pm}^2)H'_c/v^2. \quad (57)
\end{aligned}$$

In Eq. (56), $\bar{\lambda}_{ijk}$ appears six times, $\bar{\lambda}_{ijj}$ three times, and $\bar{\lambda}_{iii}$ once.

The λ_{ijkl} in Eq. (56) are the quartic scalar couplings in Eq. (13). Because of the figure-eight structure of the two-loop graphs to which they contribute ($V_{SS}^{(2)}$ in Eq. (61) below), only terms with λ_{iiii} and λ_{iiij} with $i \neq j$ in V_S are used; λ_{iiii} contributes to one term in V_S and λ_{iiij} (with $i < j$, e.g.) contributes to six terms there. They are:

$$\begin{aligned}
\lambda_{1122} &= \lambda_{1133} = \lambda_{1144} = 4M_{H'}^2 \cot^2 2\beta/v^2; \\
\lambda_{2233} &= \lambda_{2244} = \lambda_{3344} = 4M_{H'}^2 \cot^2 2\beta/v^2; \\
\lambda_{1111} &= \lambda_{2222} = \lambda_{3333} = \lambda_{4444} = 12M_{H'}^2 \cot^2 2\beta/v^2. \quad (58)
\end{aligned}$$

The two-loop effective potential in the scalar approximation is given

by [13]

$$V_2 = \kappa^2 \left(V_{SSS}^{(2)} + V_{SS}^{(2)} \right), \quad (59)$$

where, in terms of the couplings and field-dependent masses specified above:

$$V_{SSS}^{(2)} = -\frac{1}{12} \bar{\lambda}_{ijk}^2 I(\bar{M}_i^2, \bar{M}_j^2, \bar{M}_k^2), \quad (60)$$

$$V_{SS}^{(2)} = \frac{1}{8} \lambda_{iijj} J(\bar{M}_i^2, \bar{M}_j^2). \quad (61)$$

All indices on the right are summed over. The loop-integral functions $I(\bar{M}_i^2, \bar{M}_j^2, \bar{M}_k^2)$ and $J(\bar{M}_i^2, \bar{M}_j^2)$ are defined in Ref. [13]. They are symmetric under the interchange of their arguments. Therefore, there are two equal terms in $V_{SS}^{(2)}$ with λ_{iijj} with $i \neq j$. In using Martin's formulas for the I -integral, and various massless limits of it, it is important to note that the arguments are ordered as $M_i^2 \leq M_j^2 \leq M_k^2$. Martin included in the definition of these functions all factors associated with the evaluation of Feynman diagrams, including fermion-loop minus signs.¹⁹

IIIc. Numerical results for H' , A , H^\pm masses

A glance at Eqs. (49,50,51) for the CP -even masses will convince the reader that a simple, useful generalization to $\mathcal{O}(V_2)$ of the sum rule (36) is out of the question. This is so even in the approximation of keeping only the all-scalar graphs. To study the mass M_{H_2} as a function of the other scalar masses, $M_A = M_{H^\pm}$ (see footnote 2), $M_{H'}$ and M_{H_1} , we use the following algorithm:

- 1.) Increment $M_A = M_{H^\pm}$ from 180 GeV to 1 TeV.²⁰ We use $\tan \beta = 0.50$ [8].
- 2.) For each value of M_A , increment $M_{H'}$ from 10 GeV to 1 TeV.
- 3.) Calculate the $\mathcal{O}(\kappa)$ renormalization scale Λ_{GW} (Eq. (45)) and the two-loop shifts in the VEVs of H and H' .

¹⁹Only particles that become massive at tree level contribute to the figure-eight loop function $J(\bar{M}_i^2, \bar{M}_j^2)$ so that, e.g., we omitted λ_{1155} in Eqs. (58).

²⁰These are the approximate lower bound set by searches for $H^\pm \rightarrow \tau^\pm \nu_\tau$, $c\bar{b}$ and $c\bar{s}$ at LEP and the LHC and well above the upper bound of $\simeq 500$ GeV expected from the one-loop sum rule.

- 4.) Calculate the $\mathcal{O}(V_2)$ elements $(\mathcal{M}_{H_i H_j}^2)_2$ consistent with the extremal conditions solved for Λ_{GW} and $\delta_2 H'$. Then diagonalize them to $\mathcal{O}(\kappa^2)$ using Eq. (52) with δ_1 given by the $\mathcal{O}(V_1)$ approximation to Eq. (34). For comparison, we also calculated the eigenvalues and eigenvectors of $(\mathcal{M}_{H_i H_j}^2)_2$ using the approximate two-loop H - H' mixing angle δ_2 in Eq. (53). This made no discernible difference in the masses and the degree of Higgs alignment.
- 5.) We select for plotting the CP -even eigenmasses satisfying:
 - (a) The one-loop Higgs mass-squared $M_H^2 = \sum_n \alpha_n M_n^4 / 8\pi^2 v^2 > 0$.
 - (b) $(\mathcal{M}_{H' H'}^2)_2 > 0$.
 - (c) $|M_{H_1}^2 - (125 \text{ GeV})^2| \leq 1250 \text{ GeV}^2$.

These conditions always yield positive M_{H_1, H_2}^2 . For fixed M_A , the selections are usually multi-valued, satisfied for several values of $M_{H'}$. We plot the selection having M_{H_1} closest to 125 GeV. We also plot the renormalization scales Λ_0 and Λ_{GW} . As noted earlier, this procedure does not guarantee that $\det(\mathcal{M}_{0+}^2) > 0$. In this analysis, $\det(\mathcal{M}_{0+}^2) > 0$ only for $M_A < 260 \text{ GeV}$.

Figure 4 shows $M_{H'}$ vs. M_A on the left and the renormalization scales Λ_0 and Λ_{GW} on the right. There are two branches of each, $B1$ for $M_A < M_A^*(\text{pert.}) \cong 380 \text{ GeV}$ and $B2$ for $M_A > M_A^*(\text{pert.})$. On the left, the values of $M_{H'}$ for which $M_{H_1} \cong 125 \text{ GeV}$ in branch $B1$ start near 550 GeV and then rise approximately linearly with M_A to over 1 TeV. This branch ends abruptly at $M_A^*(\text{pert.})$. Branch $B2$ begins there near $M_{H'} = 0$, rising quickly and then growing linearly with M_A up to $M_A \simeq 750 \text{ GeV}$ and $M_{H'} \simeq 825 \text{ GeV}$ where the data becomes sparse because the algorithm conditions can no longer be satisfied. In branch $B1$ of the right panel, the $\mathcal{O}(\kappa)$ scale Λ_{GW} starts below Λ_0 and grows linearly with M_A , becoming almost equal to Λ_0 at $M_A \cong 260 \text{ GeV}$ for the remainder of $B1$. In branch $B2$, both scales grow linearly with M_A over the range calculated, but with a greater slope for Λ_{GW} .

Figure 5 shows $M_{H'}$ and the $\mathcal{O}(\kappa^2)$ CP -even eigenmasses M_{H_1, H_2} from $M_A = 180 \text{ GeV}$ to 750 GeV in branches $B1$ and $B2$. While $M_{H'}$ and M_{H_2} start together near 550 GeV, $M_{H'}$ grows to above 1 TeV on branch $B1$, M_{H_2} starts at $M_{H'} \cong 550 \text{ GeV}$ and grows to near 700 GeV at $M_A \cong 325 \text{ GeV}$.

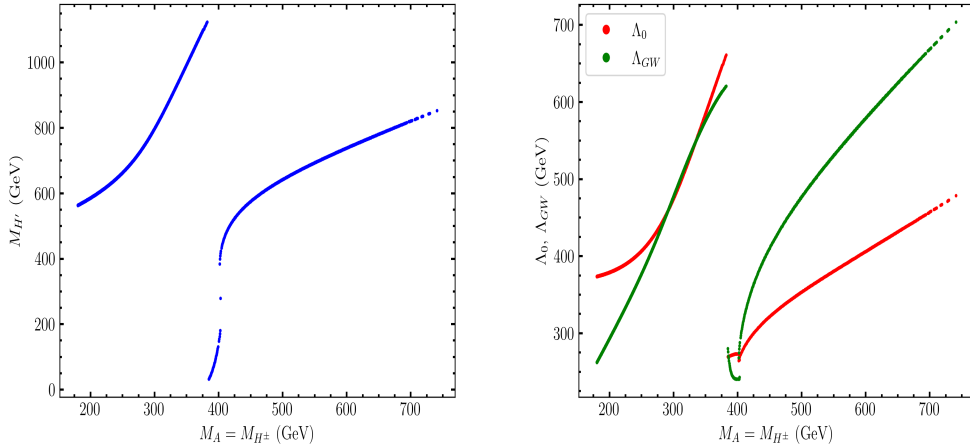


Figure 4: Left: The BSM Higgs masses $M_{H'}$ vs. $M_A = M_{H^\pm}$ with the two-loop Higgs boson mass M_{H_1} fixed near 125 GeV as described in the text. Here and below, $\tan\beta = 0.50$. Right: The renormalization scale Λ_0 (red) calculated to zero-loop order from Eqs. (25,26) and the one-loop scale Λ_{GW} (green) from Eq. (45). The two branches, $B1$ and $B2$, of $M_{H'}$ and of the renormalization scales are discussed in the text. The transition between them occurs at $M_A^*(\text{pert.}) \cong 380$ GeV.

It then drops precipitously, falling below M_{H_1} to near zero at $M_A^*(\text{pert.})$. At that point, the $B2$ branches of $M_{H'}$ and M_{H_2} emerge and grow rapidly *together* from well below M_{H_1} to about 500 GeV and, then, linearly with and approximately equal to M_A up to about 750 GeV. There is no evidence for a Higgs-like boson below 100 GeV.²¹ Also suspicious is the long linear growth with M_A of $M_{H'}$ and M_{H_2} in $B2$. For these reasons, we regard branch $B2$ as unphysical.

The behavior of M_{H_2} in branch $B1$ is similar to its one-loop approximation $\sqrt{(\mathcal{M}_{H'H'}^2)_1} \cong M_{H'}^2$ in Fig. 1. That behavior was caused by Eq. (35) for M_H^2 and its consequence, the sum rule (36) for the BSM Higgs bosons' masses. That sum rule forced $M_{H'}$ and the $\mathcal{O}(V_1)$ eigenmass M_{H_2} to be large when

²¹For a more optimistic view, see Ref. [26] and references therein.

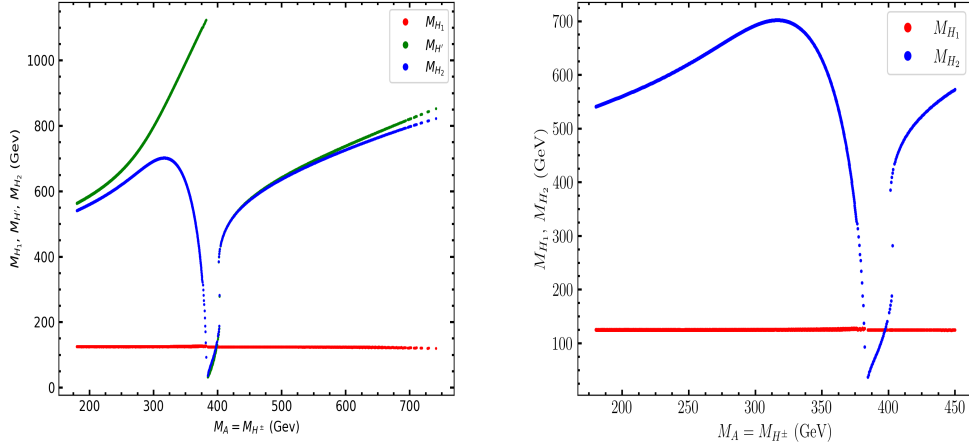


Figure 5: Left: The two-loop CP -even Higgs mass M_{H_2} with M_{H_1} fixed near 125 GeV as described in the text. The input $M_{H'}$ is shown for comparison with M_{H_2} . The $B1$ – $B2$ transition between the two branches of M_{H_2} vs. M_A occurs at $M_A^*(\text{pert.}) \cong 380$ GeV. Right: A close-up of the $B1$ – $B2$ transition region

M_{A,H^\pm} were near the experimental lower bound of 180 GeV for M_{H^\pm} and, then, to plunge to zero when $(M_A^4 + 2M_{H^\pm}^4)^{-1/4} \rightarrow 540$ GeV.

A similar thing is happening here: setting $M_{H_1} \cong 125$ GeV is a strong constraint on the BSM Higgs masses, although its mechanics are less obvious. First, $(\mathcal{M}_{HH}^2)_2$ in Eq. (49) is dominated by its first and third terms, the one-loop Higgs mass, $M_H^2 = \sum_n \alpha_n M_n^4 / 8\pi^2 v^2$, and $(\partial V_2 / \partial H^2)_{\langle \rangle}$. The condition $M_H^2 > 0$ requires $M_{H'}^4 + M_A^4 + 2M_{H^\pm}^4 > 12M_t^4 \simeq 10^{10} \text{ GeV}^4 (\gg 6M_W^4 + 3M_Z^4)$. This favors large BSM masses, and as M_{A,H^\pm} increase, so does $M_{H'}$ which is being forced to be large by the algorithm's conditions (5b,c). Thus, the M_{H_1} constraint requires $(\partial V_2 / \partial H^2)_{\langle \rangle} < 0$ and increasing in magnitude.

The other feature of Fig. 5 in common with the one-loop masses in Fig. 1 is M_{H_2} falling from its maximum value to near zero at the $B1$ – $B2$ transition at $M_A^*(\text{pert.})$. The dominant terms at large BSM masses in Eq. (51) are $M_{H'}^2 > 0$ and the last two, $(-6 \cot 2\beta / v)(\partial V_2 / \partial H')_{\langle \rangle} < 0$ and $(\partial^2 V_2 / \partial H'^2)_{\langle \rangle} > 0$. All

three terms are large and there is a tug-of-war between the latter two which the negative term wins, driving $M_{H_2} \cong \sqrt{(\mathcal{M}_{H'H'}^2)_2}$ below 125 GeV — a level *crossing* between the two CP -even eigenvalues. This is the same as its behavior in Figs. 1. Recall that, in that figure and this one, the diagonalization of \mathcal{M}_{0+}^2 was carried out strictly to $\mathcal{O}(V_1)$ and $\mathcal{O}(V_2)$, respectively, by omitting or truncating the off-diagonal $\mathcal{M}_{HH'}^2$ term.²²

The one and two-loop H – H' mixing angles are negative and nearly equal to each other, $\delta_1 \cong \delta_2 \cong -0.001$ for $180 \text{ GeV} < M_A \lesssim 350 \text{ GeV}$. Above 350 GeV δ_2 decreases rapidly to -0.028 at $M_A \cong M_{A^*} = 380 \text{ GeV}$ because the denominator $(\mathcal{M}_{H'H'}^2 - \mathcal{M}_{HH}^2)_2 \cong M_{H_2}^2 - M_{H_1}^2$ of $\tan 2\delta_2$ is becoming smaller as the $B1$ – $B2$ transition is approached; see Fig. 5.

The experimental consequences of the perturbative method are presented in Sec. IV.

III. The GW-2HDM model at two-loops: the amoeba method

In this section we use a different method to calculate the eigenmasses and eigenvectors of the CP -even scalars H and H' . The results of this calculation and the one in Sec. II are similar. The reasons for this and for their differences will be explained. In this method, the potential $V_{\text{eff}} = V_0 + V_1 + V_2$ for the GW-2HDM is a function of: $\tan \beta = v_2/v_1$, the ratio of the VEVs of the CP -even components of the complex Higgs doublets Φ_2 and Φ_1 ; the BSM Higgs masses M_A , M_{H^\pm} and $M_{H'}$;²³ the classical fields H_c and H'_c corresponding to the VEVs of the aligned-basis fields H and H' ; and the renormalization scale Λ_{GW} .

We fix $\tan \beta = 0.50$, the experimental upper limit from the searches by

²²In Sec. III, the same dive of M_{H_2} occurs at the $B1$ – $B2$ transition, but a level *repulsion*, not a level crossing, occurs there because the full $\mathcal{M}_{HH'}^2$ is included in diagonalizing \mathcal{M}_{0+}^2 — as was done in Fig. 2.

²³Recall that the tree-approximation extremal conditions remain in force which, with $\tan \beta$, reduce the number of independent quartic couplings to three, namely, λ_5 , λ_{45} and λ_{345} . We also remind the reader that an upper limit on $\tan \beta$ in this model is a lower limit on $\tan \beta$ in the usual 2HDM's with natural flavor conservation [12].

CMS [19] and ATLAS [20] for $gg \rightarrow t\bar{b}H^- \rightarrow t\bar{t}b\bar{b}$ for $180 \text{ GeV} < M_{H^\pm} \lesssim 500 \text{ GeV}$. We also adopt the precision electroweak constraint $M_A = M_{H^\pm}$ [14, 15, 16], and we assume that $M_{H',A,H^\pm} \lesssim \mathcal{O}(1 \text{ TeV})$, a conservative upper limit suggested by the analyses of Secs. I and II.

The program *Amoeba* [24] is used to minimize V_{eff} with respect to H_c and H'_c subject to the constraint,

$$H_c^2 + H'_c{}^2 = v^2 = (246.2 \text{ GeV})^2, \quad (62)$$

and with respect to Λ_{GW} .²⁴ This procedure is carried out for BSM masses below 1 TeV. Its outputs are the renormalization scale Λ_{GW} , the VEV shift H'_c (with the corresponding shift in H_c dictated by Eq. (62)), and the eigenvalues M_{H_1,H_2} and eigenvectors H_1, H_2 of the CP -even mass matrix. Minimization of V_{eff} requires that \mathcal{M}_{0+}^2 is a positive-definite matrix. This is not yet enough to realistically fix M_{H_1,H_2} , H_1, H_2 , and Λ_{GW} . That happens when we require that one of the CP -even eigenmasses is $M_H = 125 \text{ GeV}$. We refer to this procedure as the “amoeba method”.

The regions of stability of the one- and two-loop effective potentials for BSM Higgs masses below 1 TeV are shown in Figs. 6. Except for the small top-quark terms in V_1 , the one-loop potential is a function of H_c and H'_c only through $H_c^2 + H'_c{}^2 = v^2$ and, so, it is nearly independent of them. This accounts for its large region of stability below 1 TeV. The small hole near the origin of this plot occurs because Eq. (35) cannot be satisfied for $M_H^2 > 0$ for that region of BSM masses. The cubic and quartic couplings that enter V_2 constrain the region of stability of the full two-loop potential to $300 \text{ GeV} \lesssim M_A = M_{H^\pm} \lesssim 900 \text{ GeV}$ and $25 \text{ GeV} \lesssim M_{H'} \lesssim 900 \text{ GeV}$. The mass scale of these ranges is set by $v = 246 \text{ GeV}$, of course. From now on, we require that *one of the CP-even eigenmasses* $M_{H_1,H_2} = M_H = 125 \text{ GeV}$. We will see that only the case $M_{H_1} = 125 \text{ GeV}$ is allowed experimentally.

Most notably, the amoeba method differs from the perturbative one in that \mathcal{M}_{0+}^2 is required to be positive-definite. Its determinant therefore contains terms of order three and four loops ($\mathcal{O}(\kappa^3)$ and $\mathcal{O}(\kappa^4)$). Furthermore,

²⁴Because of the constraint (62), this minimization involves two independent parameters, as in the perturbative method.

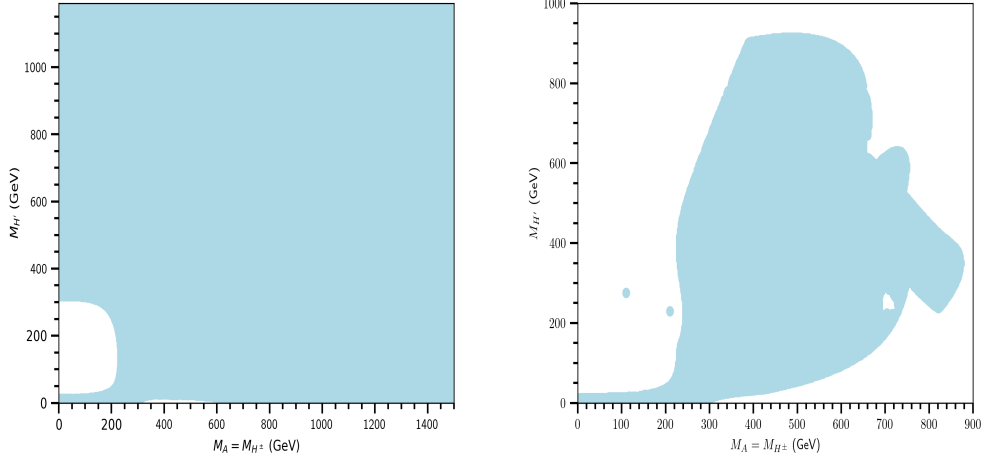


Figure 6: Left: The region (shown in blue) of $0 < M_A = M_{H^\pm} < 1450$ GeV and $0 < M_{H'} < 1200$ GeV for which the one-loop effective potential $V_0 + V_1$ has a minimum as described in the text. Right: The Mr. Magoo region (in blue) for which the two-loop potential $V_0 + V_1 + V_2$ has a minimum for the same ranges of $M_A = M_{H^\pm}$ and $M_{H'}$. The Higgs mass M_{H_1} has not been fixed at 125 GeV in these plots.

its eigenvectors and eigenmasses also contain terms of $\mathcal{O}(\kappa^3)$ and $\mathcal{O}(\kappa^4)$:

$$\begin{aligned} H_1 &= H \cos \delta - H' \sin \delta, \\ H_2 &= H \sin \delta + H' \cos \delta, \end{aligned} \quad (63)$$

$$\begin{aligned} M_{H_1}^2 &= \mathcal{M}_{H_c H_c}^2 \cos^2 \delta + \mathcal{M}_{H'_c H'_c}^2 \sin^2 \delta - 2\mathcal{M}_{H_c H'_c}^2 \sin \delta \cos \delta, \\ M_{H_2}^2 &= \mathcal{M}_{H_c H_c}^2 \sin^2 \delta + \mathcal{M}_{H'_c H'_c}^2 \cos^2 \delta + 2\mathcal{M}_{H_c H'_c}^2 \sin \delta \cos \delta, \end{aligned} \quad (64)$$

where, now, the H - H' mixing angle δ is obtained from the ratio of derivatives with respect to H_c and H'_c of the full two-loop V_{eff} :

$$\tan 2\delta = \frac{2\mathcal{M}_{H_c H'_c}^2}{\mathcal{M}_{H'_c H'_c}^2 - \mathcal{M}_{H_c H_c}^2}. \quad (65)$$

Since V_{eff} depends on the “tree-level” BSM Higgs masses, $M_A = M_{H^\pm}$ and

$M_{H'}$ in Eq. (8), this procedure also determines the allowed ranges of those masses.

As an application of the amoeba method, one that highlights its difference from the perturbative method of Secs. I and II, we apply it to the one-loop potential V_0+V_1 , requiring that the lighter eigenvalue of \mathcal{M}_{0+}^2 equals 125 GeV. The square roots of the elements of the one-loop \mathcal{M}_{0+}^2 are shown in the left panel of Fig. 7. For $M_A = M_{H^\pm} \lesssim 410$ GeV, note how small the off-diagonal $\sqrt{|\mathcal{M}_{H_c H_c'}^2|}$ is compared to the diagonal elements. This is the hallmark of Higgs alignment in this approximation of the GW-2HDM, in particular, that $\sqrt{\mathcal{M}_{H_c H_c}^2} \cong M_{H_1} = 125$ GeV and $\sqrt{\mathcal{M}_{H_c' H_c'}^2} \cong M_{H_2} > 125$ GeV. Also, the BSM masses satisfy the sum rule Eq. (36), which is built into V_1 .²⁵ Here, the important difference with the perturbative method is the appearance of the small contribution $\pm 2\mathcal{M}_{H_c H_c'}^2 \sin \delta \cos \delta$ in Eqs. (64). This term was excluded in Sec. I because it is $\mathcal{O}(\kappa^2)$. It effects the eigenvalues of \mathcal{M}_{0+}^2 only very near $M_A = 410$ GeV — where the denominator of $\tan 2\delta$ is vanishing. In Fig. 1, the region $M_A > 410.5$ GeV is unphysical because it violates the sum rule, and the curves end there. In the amoeba method, the $\sqrt{\mathcal{M}_{H_c H_c}^2}$ and $\sqrt{\mathcal{M}_{H_c' H_c'}^2}$ curves cross at $M_A = 410.5$ GeV and $\sqrt{\mathcal{M}_{H_c H_c}^2}$ rises approximately linearly while $\sqrt{\mathcal{M}_{H_c' H_c'}^2} = 125$ GeV.²⁶ As in the perturbative method, this region is unphysical; i.e., even in one loop of the amoeba method there are two branches with the transition at the sum-rule cutoff of 410.5 GeV.

Another difference between the two methods is that, in the perturbative one, the two-loop effective potential in $B1$ is very well-approximated by its all-scalar terms with the cracked-egg (SSS) contribution alone accounting for 98% of the total; see Fig. 3. That simplification does not occur in the amoeba method. It appears to be due to the different regimes of BSM Higgs masses M_A and $M_{H'}$ that give acceptable solutions for M_{H_1, H_2} in the two methods. In the perturbative method, $M_{H'}$ increases from 550 GeV to 700 GeV and then

²⁵This calculation covered $M_{A, H^\pm} = 0$ to 600 GeV, endpoints outside the range of the experimental lower bound on M_{H^\pm} and the one-loop sum rule, but for which V_{eff} has a stable minimum.

²⁶This is *not* a level crossing. In fact, the *eigenvalues* repel each other there as can be seen in Fig. 10 for the two-loop masses.

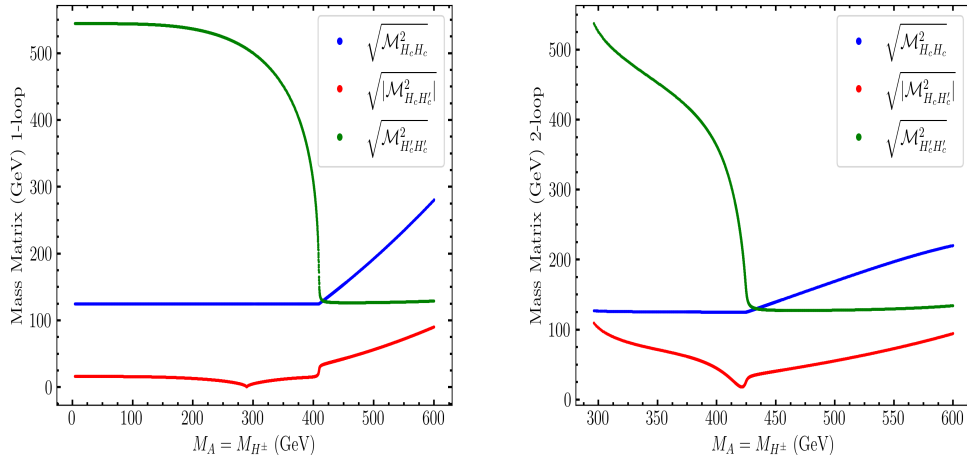


Figure 7: The square roots of the elements of \mathcal{M}_{0+}^2 in the amoeba method for the one-loop effective potential (left) and the two-loop effective potential (right). The lighter CP -even eigenvalue is required to be 125 GeV here.

falls to below 125 GeV for $180 \text{ GeV} < M_A < M_A^*(\text{pert.}) = 380 \text{ GeV}$. In the amoeba method, the ranges are $550 \text{ GeV} > M_{H'} > 125 \text{ GeV}$ for $290 \text{ GeV} < M_A < M_A^*(\text{amoe.}) = 425 \text{ GeV}$. We shall see that the region of V_{eff} -stability in which the *lighter* CP -even eigenvalue $M_{H_1} = 125 \text{ GeV}$ will divide into two branches, $B1$ and $B2$, with physically acceptable results only in $B1$ — as in the perturbative method. In $B1$, the ratios to the cracked-egg all-scalar contribution of several other contributions to the two-loop potential are not very small. The sum of the ratios of the other contributions to SSS is typically 10–50%, with the largest contributions after SSS being SSV, FFV and SS; see Fig. 8. Note that none of these next-largest contributions have field-dependent couplings; see Ref. [13] for details of these potentials.

The left panel of Fig. 9 shows the one- and two-loop renormalization scale Λ_{GW} over the ranges of the $\sqrt{\mathcal{M}_{0+}^2}$ in Fig. 7; $M_{H_1} = 125 \text{ GeV}$ is the lighter CP -even eigenvalue in both curves. The magnitudes of these renormalization scales are comparable to those of the two-loop scales Λ_0 and Λ_{GW} in the perturbative method (Fig. 4, right panel), their values again being set by

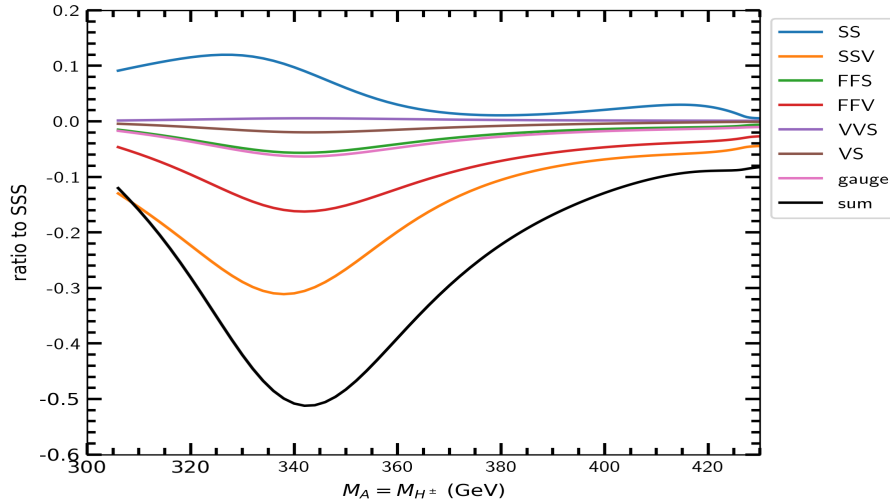


Figure 8: Ratios to the SSS cracked-egg contribution of the SS figure-eight, SSV, FFS, FFV, VVS, VS figure-eight, and gauge contributions to V_2 for $290 \text{ GeV} \lesssim M_A = M_{H^\pm} \lesssim M_A^*(\text{amoeba}) = 425 \text{ GeV}$, the $B1$ -branch region of the left panel of Fig. 10. The black curve is the sum of the eight ratios. $M_{H_1} = 125 \text{ GeV}$ is the lighter CP -even eigenvalue here. In addition to V_{SSS} and V_{SS} , these two-loop potentials are taken from Martin [13].

$v = 246 \text{ GeV}$. But, while the renormalization scales in the perturbative method are discontinuous at the $B1$ – $B2$ transition (as is $M_{H'}$), the transitions in the amoeba method are continuous (again, as is $M_{H'}$ in the left panel of Fig. 10), albeit with slight changes of slope.

The right panel of Fig. 9 is more interesting: $H_c \cong 246 \text{ GeV}$ in $B1 = 290$ – 425 GeV and decreasing only slightly in $B2 = 425$ – 600 GeV ; H'_c is negligibly small in $B1$ (alignment again), but jumps to 20 GeV at the transition and increases with M_A from there up to $M_A = 600 \text{ GeV}$. Stable solutions of V_{eff} are scarce beyond this upper limit of $B2$.

Finally, we extract the CP -even masses and states. The two possibilities for which eigenmass is 125 GeV are shown in Figs. 10. The masses $M_{H'}$, M_{H_1} , M_{H_2} and the complete two-loop H – H' mixing angle δ are plotted vs. $M_A =$

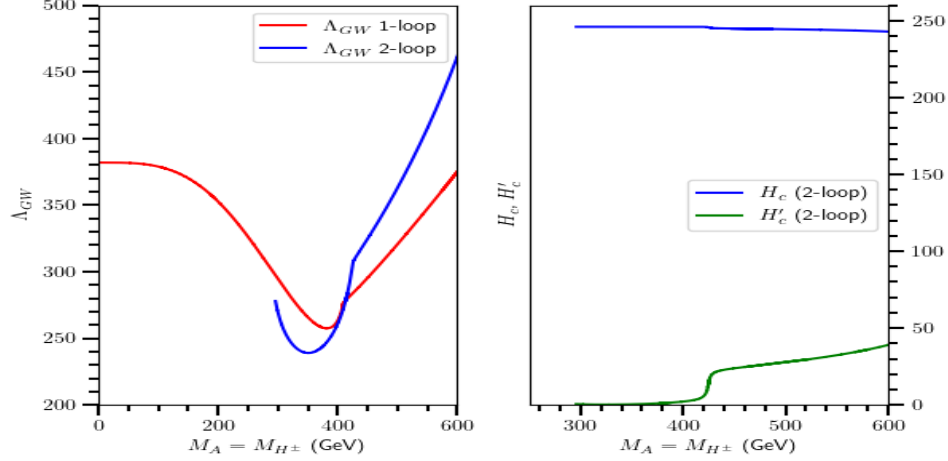


Figure 9: Left: The renormalization scale Λ_{GW} in the one- and two-loop approximations of the amoeba method. They are plotted over the ranges of the $B1$ and $B2$ branches in the left panel of Fig. 10. Note the slight discontinuity in their slopes at the transition between the two branches at 425 GeV. Right: The classical-field shifts H_c and H'_c at the minima of the two-loop V_{eff} as a function of $M_A = M_{H^\pm}$. The smallness of H'_c , especially in branch $B1$, is a consequence of the requirement that $\mathcal{M}_{H_c H'_c}^2$ is small enough that $\det \mathcal{M}_{0+}^2 > 0$.

M_{H^\pm} for the regions in which V_{eff} has a stable minimum.²⁷ Clearly, only the case that $M_{H_1} = 125$ GeV is consistent with light Higgs-boson searches from LEP and LHC. In the left panel, M_{H_2} and $M_{H'}$ decrease from 550 GeV to just above and below $M_{H_1} = 125$ GeV, and they are indistinguishable up to $M_A \cong M_A^*(\text{amoe.}) = 425$ GeV. As the right panel of Fig. 7 and this figure illustrate, this is due to the smallness of $\delta \cong \mathcal{M}_{H_c H'_c}^2 / (\mathcal{M}_{H'_c H'_c}^2 - \mathcal{M}_{H_c H_c}^2)$ for $M_A < M_A^*(\text{amoe.})$. At $M_A^*(\text{amoe.})$, where δ passes rapidly from near zero to $\pi/4$, there is a level repulsion between M_{H_2} and M_{H_1} .²⁸ Beyond that point,

²⁷When $M_{H_2} = 125$ GeV, it is difficult to obtain a stable minimum of V_{eff} above $M_A \cong 400$ GeV.

²⁸This is the same behavior as the one-loop eigenmasses and the $H-H'$ mixing angle in

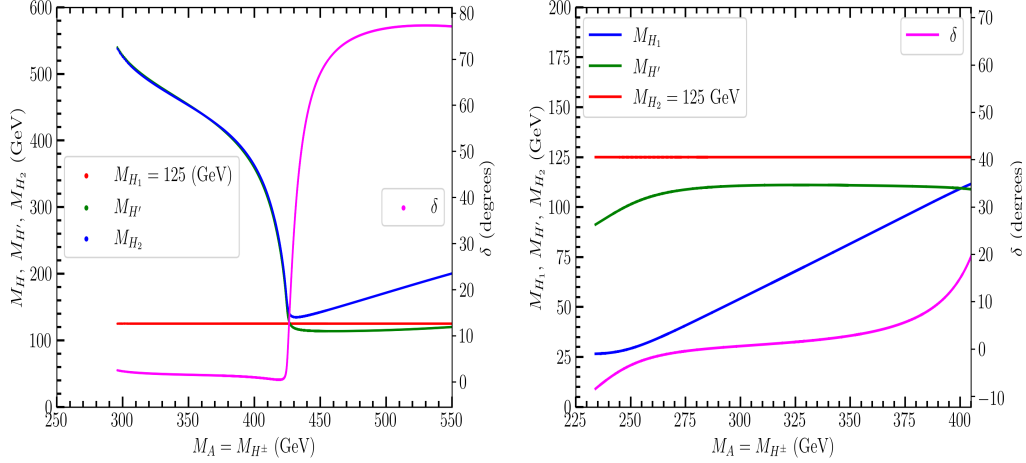


Figure 10: Left: The BSM Higgs masses for the case that the smaller CP -even eigenmass is $M_{H_1} = 125$ GeV. Also shown (in magenta) is the *full two-loop* $H-H'$ mixing angle (in degrees) obtained from Eq. (34). Right: The BSM Higgs masses and two-loop $H-H'$ mixing angle when the larger CP -even eigenmass is $M_{H_2} = 125$ GeV.

M_{H_2} rises linearly with M_A and $M_{H'}$ crosses M_{H_1} but remains nearly equal to it. Furthermore, the large value of δ violates loop perturbation theory. As in the perturbative method for the two-loop potential, there are two branches of M_{H_2} , the physical one $B1$ below M_A^* (amoeba) and the unphysical one $B2$ above it.

It is interesting to compare the masses in the perturbative method, Fig. 5, with those here in the amoeba method. The behaviors of $M_{H'}$ in the two methods are radically different, increasing rapidly in both branches with a jump discontinuity at the transition in the first method, while decreasing to $M_{H_1} = 125$ GeV in the second. On the other hand, the behaviors of M_{H_2} in the two methods are strikingly similar. In $B1$, it starts near 550 GeV, its maximum value in the second method, not far below its maximum of 700 GeV in the first one. Then, in both methods, it dives to well below or just below

the right panel of Fig. 2.

$M_{H_1} = 125$ GeV at the $B1$ – $B2$ transition. In $B2$, M_{H_2} grows linearly with $M_A = M_{H^\pm}$ in both methods. In the perturbative method calculation, M_A runs over the range 180–1100 GeV, but it is clear in Fig. 5 that the criteria for generating M_{H_1} and M_{H_2} are difficult to meet above $M_A = 700$ GeV. This is similar to the upper limit $M_A = 600$ – 700 GeV in the region of stability of the two-loop potential in Fig. 6.

IV. Experimental consequences for the GW-2HDM in two loops

We have stressed that the only feasible way of testing the GW-2HDM (and similar GW models) in the foreseeable future is to discover or exclude its BSM Higgs bosons H_2 , A , H^\pm .²⁹ As in the one-loop analysis, the overriding features of these bosons are (1) their low masses, well below 1 TeV, and (2) the high degree of alignment of the 125 GeV Higgs boson H and the related strong suppression of the BSM bosons' couplings to W^+W^- , ZZ , $W^\pm Z$ and ZH , $W^\pm H$. Additional suppression in their production rates is due to the appearance in their Yukawa couplings of $\tan\beta \lesssim 0.50$ for $M_{H^\pm} \lesssim 500$ GeV. This section summarizes the BSM Higgs mass ranges found in our two-loop calculations, their couplings to electroweak gauge bosons and to quarks and leptons, and the searches we believe are likely to reveal, or exclude, the BSM Higgses.³⁰

The BSM masses obtained in our two-loop study are qualitatively similar to those found using the simple one-loop sum rule in Eq. (36) and, as we have discussed, for much the same reason, namely, the constraint on these masses from the requirement that $M_H = 125$ GeV. As explained in Sec. I, we require $M_{H^\pm} \geq 180$ GeV and $M_A = M_{H^\pm}$. Then, the physical (branch

²⁹In this section, we use H and H_1 interchangeably because, as we saw in the amoeba method, only the lightest CP -even eigenvalue $M_{H_1} = 125$ GeV is consistent with Higgs boson searches near and below that mass. We do not use H' and H_2 interchangeably because of their very different dependence on M_{A,H^\pm} in the perturbative method.

³⁰Earlier discussions of the BSM Higgs searches for masses in the one-loop approximation are in Refs. [8, 10, 11].

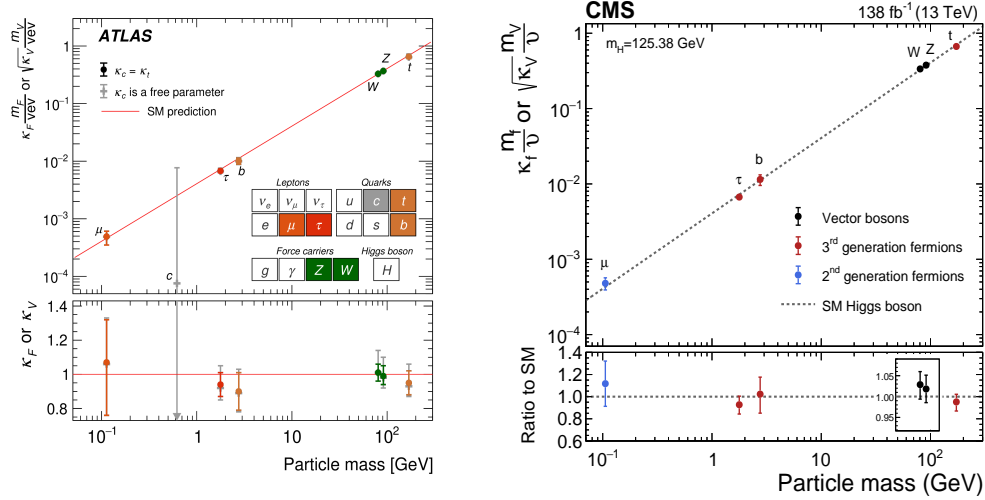


Figure 11: The mass-dependent couplings of the 125-GeV Higgs boson H to quarks, leptons and the W and Z determined by ATLAS [27] and CMS [28] from their full LHC Run 2 data sets. The lower panel in each figure is the ratio of the measured couplings to the Standard Model ones.

B1) BSM mass ranges are (from Figs. 5,10):

$$\begin{aligned}
 180 \text{ GeV} &\lesssim M_A = M_{H^\pm} \lesssim 380 \text{ GeV}, \\
 700 \text{ GeV} &\gtrsim M_{H_2} \gtrsim 125 \text{ GeV} \quad (\text{perturbative method}); \quad (66)
 \end{aligned}$$

$$\begin{aligned}
 290 \text{ GeV} &\lesssim M_A = M_{H^\pm} \lesssim 425 \text{ GeV}, \\
 550 \text{ GeV} &\gtrsim M_{H_2} \gtrsim 125 \text{ GeV} \quad (\text{amoeba method}). \quad (67)
 \end{aligned}$$

These ranges are correlated, with M_{H_2} decreasing as $M_A = M_{H^\pm}$ increase. As in the one-loop analysis, M_{H_2} decreases to unrealistically small values as $M_A = M_{H^\pm}$ increase to their maximum allowed (M_A^*) by the method used.

The degree of Higgs alignment is dramatically illustrated in Figs. 11. These are the full Run 2 determinations of the couplings of H to quarks, leptons and weak bosons from ATLAS [27] and CMS [28]. All the measurements are within one standard deviation of the Standard Model prediction. From a theoretical point of view, the 125 GeV Higgs boson is either the lone ‘‘Higgs’’

of the Standard Model [29, 30, 31, 32, 33, 34, 35] or Higgs alignment [2, 3, 4] is verified experimentally.

The allowed and strongly suppressed couplings in the GW-2HDM, are in the interaction \mathcal{L}_{EW} of the Higgs bosons with the electroweak gauge bosons [8]. Having found that the H - H' mixing angle $\delta \lesssim \mathcal{O}(10^{-2})$ through two-loop order, an excellent approximation to \mathcal{L}_{EW} is obtained by putting $\sin \delta = 0$, $H = H_1$ and $H' = H_2$:

$$\begin{aligned}
\mathcal{L}_{EW} &= ieH^- \overleftrightarrow{\partial}_\mu H^+ (A^\mu + Z^\mu \cot 2\theta_W) + \frac{e}{\sin 2\theta_W} (H_2 \overleftrightarrow{\partial}_\mu A) Z^\mu \\
&+ \frac{ig}{2} \left(H^+ \overleftrightarrow{\partial}_\mu (H_2 + iA) W^{-\mu} - H^- \overleftrightarrow{\partial}_\mu (H_2 - iA) W^{+\mu} \right) \\
&+ H_1 \left(gM_W W^{+\mu} W_\mu^- + \frac{1}{2} \sqrt{g^2 + g'^2} M_Z Z^\mu Z_\mu \right) + \\
&+ (H_1^2 + H_2^2 + A^2) \left(\frac{1}{4} g^2 W^{+\mu} W_\mu^- + \frac{1}{8} (g^2 + g'^2) Z^\mu Z_\mu \right) \\
&+ H^+ H^- \left(e^2 (A_\mu + Z_\mu \cot 2\theta_W)^2 + \frac{1}{4} g^2 W_\mu^+ W^{-\mu} \right), \quad (68)
\end{aligned}$$

where $\tan \theta_W = g'/g$ and $e = gg'/\sqrt{g^2 + g'^2}$. The negative results of LHC searches for the 2HDM Higgs bosons H_2 , A and H^\pm are entirely consistent with Eq. (68); see <https://twiki.cern.ch/twiki/bin/view/AtlasPublic> and <https://cms-results.web.cern.ch/cms-results/public-results/publications>.

Another, less dramatic but possibly important, suppression due to $\tan \beta \lesssim 0.50$ is in the fermions' Yukawa interaction. Because of alignment and our choice in Eq. (4) of the type-I model for the GW-2HDM, all the BSM Higgs couplings to quarks and leptons are proportional to $\tan \beta$:³¹

$$\begin{aligned}
\mathcal{L}_Y &= \frac{\sqrt{2} \tan \beta}{v} \sum_{k,l=1}^3 [H^+ (\bar{u}_{kL} V_{kl} m_{d_l} d_{lR} - \bar{u}_{kR} m_{u_k} V_{kl} d_{lL} + m_{\ell_k} \bar{\nu}_{kL} \ell_{kR} \delta_{kl}) + \text{h.c.}] \\
&- \left(\frac{v + H_1 - H_2 \tan \beta}{v} \right) \sum_{k=1}^3 (m_{u_k} \bar{u}_k u_k + m_{d_k} \bar{d}_k d_k + m_{\ell_k} \bar{\ell}_k \ell_k) \\
&- \frac{iA \tan \beta}{v} \sum_{k=1}^3 (m_{u_k} \bar{u}_k \gamma_5 u_k - m_{d_k} \bar{d}_k \gamma_5 d_k - m_{\ell_k} \bar{\ell}_k \gamma_5 \ell_k), \quad (69)
\end{aligned}$$

³¹Hence the upper limit $\tan \beta \lesssim 0.50$ from the LHC searches for H^\pm . In the conventional definition of the type-I 2HDM [12], the analysis in Ref. [8] would have found $\cot \beta \lesssim 0.50$, in significant contradiction, e.g., with the experimental limits [36, 37] discussed below.

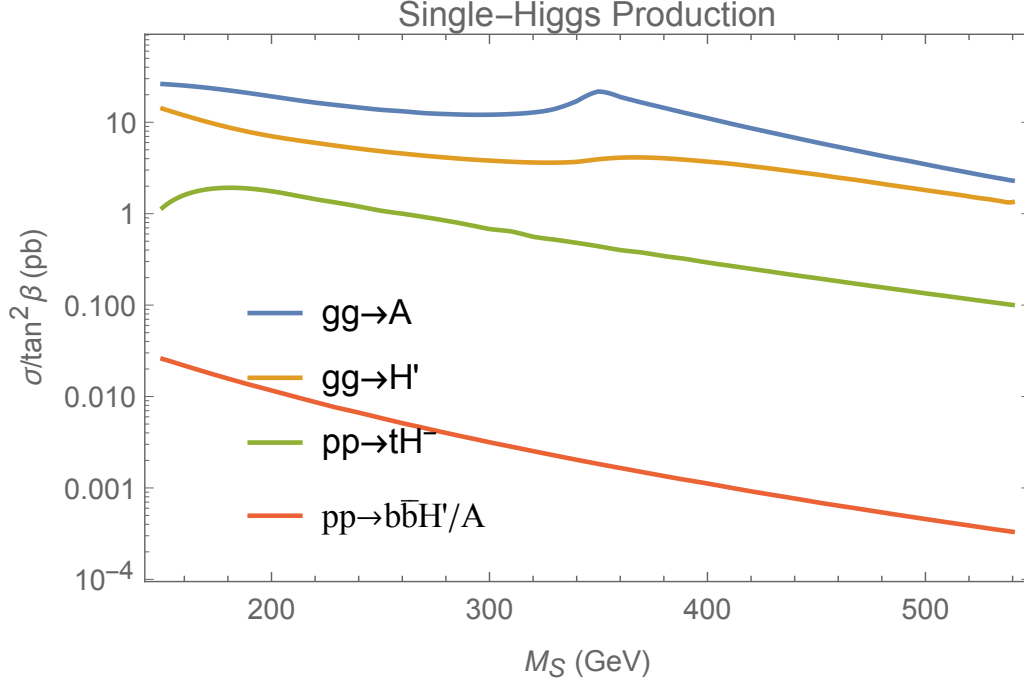


Figure 12: The gluon fusion cross sections for $\sqrt{s} = 13$ TeV at the LHC for single BSM Higgs production in the alignment limit ($\delta \rightarrow 0$) of the GW-2HDM [8]. The dependence on $\tan\beta$ has been scaled out; both charged Higgs states are included in $pp \rightarrow t\bar{b}H^-$.

where $V = U_L^\dagger D_L$ is the CKM matrix. The cross sections for gluon fusion (with $\tan^2\beta$ scaled out) and for Drell-Yan production of the BSM bosons at the 13 TeV LHC are shown in Figs. 12 and 13. Except at low $M_A = M_{H^\pm}$ or $\tan\beta \lesssim 0.1$, the gluon fusion rates are typically $\gtrsim 100$ times larger than Drell-Yan ones.

Thus, the most common production processes of the BSM scalars in the GW-2HDM are:

$$gg \rightarrow b\bar{b} \rightarrow t\bar{b}H^- + \text{c.c.}, \quad (70)$$

$$gg \rightarrow t\bar{t} \rightarrow H_2, A. \quad (71)$$

The process (71) may go through a top-quark loop or via on-shell tops with four top quarks in the final state if M_{H_2} or $M_A > 2m_t$; both possibilities are

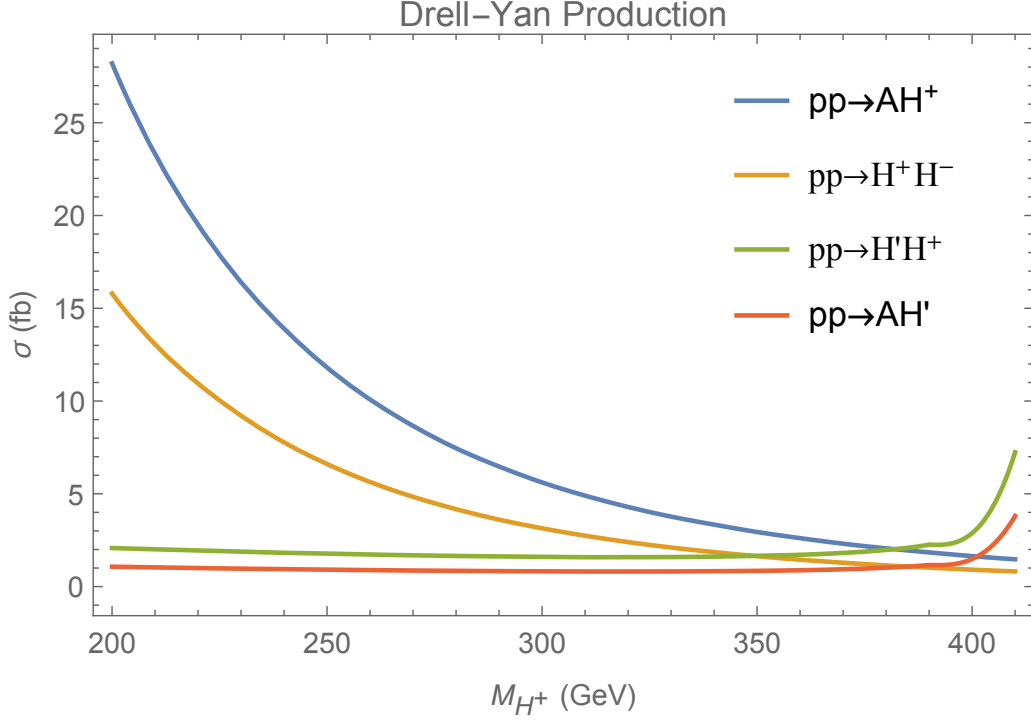


Figure 13: The Drell-Yan cross sections for $\sqrt{s} = 13$ TeV at the LHC for production of Higgs pairs in the alignment limit ($\delta \rightarrow 0$) [8]. They are independent of $\tan\beta$. $M_{H^\pm} = M_A$ is assumed, with M_{H_2} taken from Eq.(36). The sharp increase at large M_{H^\pm} is due to the rapid decrease of M_{H_2} there.

discussed below. The rate for the common search mode $gg \rightarrow H_2, A \rightarrow \gamma\gamma$ via a top loop is suppressed by $\tan^2\beta$ as well as having the usual small $\mathcal{O}(\alpha^2)$ branching ratio.

For the two-loop mass ranges in Eqs. (66, 67) the major BSM decay modes are:³²

$$H^+ \rightarrow t\bar{b}; \quad (72)$$

$$A \rightarrow b\bar{b}, \tau^+\tau^-, t\bar{t}; \quad (73)$$

$$H_2 \rightarrow b\bar{b}, \tau^+\tau^-, t\bar{t} \text{ and } ZA, W^\pm H^\mp. \quad (74)$$

Since $M_A = M_{H^\pm}$ must be about 100 GeV greater than M_{H_2} to enable the

³²The assumption $M_{H^\pm} = M_A$ precludes $A \rightarrow W^\pm H^\mp$.

decays $H^\pm \rightarrow W^\pm H_2$ and $A \rightarrow ZH_2$, they are forbidden in the two-loop mass ranges found with the perturbative method. In the amoeba method, these decays are allowed only for $M_{A,H^\pm} = 410\text{--}425$ GeV, with rates much smaller than $H^+ \rightarrow t\bar{b}$ and $A \rightarrow t\bar{t}$.³³

We focus on three types of BSM Higgs production and decay:

- 1.) $gg \rightarrow H^\pm \bar{t}b \rightarrow t\bar{t}b\bar{b}$ and $gg \rightarrow H_2 \rightarrow W^\pm H^\mp \rightarrow W^\pm \bar{t}b$

There have been five searches for the first process relevant to the mass range of the GW-2HDM [19, 20, 38, 39, 40]. The first of these was a CMS search at 8 TeV; the other four used 13 TeV data. Ref. [39] is an ATLAS search using its full Run 2 data set of 139 fb^{-1} . Ref. [40] is a CMS search using 35.9 fb^{-1} of 13 TeV data taken in 2016; it is distinguished by having looked for the $\bar{t}b\bar{b}$ final state in the all-jet mode.

The 8 TeV search by CMS [19] was used in Ref. [8] to set the limit $\tan\beta \lesssim 0.50$ for $180\text{ GeV} < M_{H^\pm} \lesssim 500\text{ GeV}$. The searches at 13 TeV have not improved on this limit despite the larger data sets and, indeed, they have worse sensitivity at $M_{H^\pm} = 200\text{--}500$ GeV than the CMS 8-TeV result. For example, the limit on $\tan\beta$ for $M_{H^\pm} = 200\text{--}500$ GeV extracted from the ATLAS 139 fb^{-1} data [39] is $\tan\beta < 1.10 \pm 0.14$ [11]. The reason for this disappointing outcome is the large $t\bar{t}$ background at low masses and the fact that it increases with collider energy faster than the signal.

Given the payoff a significant improvement in the limit on $\tan\beta$ at low M_{H^\pm} might have, we strongly urge ATLAS and CMS to find a way to improve the signal efficiency of this search. One possibility may be to use

$$gg \rightarrow H_2 \rightarrow W^\pm H^\mp. \quad (75)$$

Since H^+ decays to $t\bar{b}$, the final state in this mode, $W^+W^-b\bar{b}$, is the same as the near-threshold process above. But, because it occurs at a higher invariant mass, kinematic cuts taking advantage of

³³In the one-loop approximation, these decays are allowed, but only for $400\text{ GeV} \lesssim M_A = M_{H^\pm} \lesssim 410\text{ GeV}$ and for $M_{H_2} \gtrsim 450\text{ GeV}$ [10, 11]. The decays $H_2 \rightarrow W^\pm H^\mp$ and ZA with two-loop-masses are discussed below.

that may provide a better signal-to-background ratio. The H_2 decay rate is proportional to p_W^3 and, therefore, is sensitive to the available phase space. It quickly becomes dominant when $M_{H_2} \gtrsim 400$ GeV and the W is longitudinally polarized.³⁴ In the perturbative calculation of the two-loop BSM masses practically the entire allowed range of M_{H^\pm} is covered — from 180 GeV to 365 GeV, with M_{H_2} ranging from 540 GeV up to 700 GeV and back down to 510 GeV. In the amoeba method, the allowed region is restricted to $M_{H^\pm} = 300\text{--}350$ GeV, with $M_{H_2} = 525$ GeV down to 450 GeV.³⁵

2.) $gg \rightarrow A/H_2 \rightarrow t\bar{t}$ and $gg \rightarrow t\bar{t} \rightarrow t\bar{t}A/H_2 \rightarrow t\bar{t}t\bar{t}$

A search by CMS with 35.9 fb^{-1} of data at 13 TeV for $\varphi = A/H_2 \rightarrow t\bar{t}$ with low mass, $400 < M_{A/H_2} < 750$ GeV, is in Ref. [42]. Gluon fusion production proceeds through a top loop, and the principal background is $gg \rightarrow t\bar{t}$ near threshold. CMS presented model-independent constraints on the “coupling strength” $g_{\varphi t\bar{t}} = \lambda_{\varphi t\bar{t}}/(M_t/v)$ and for width-to-mass ratios $\Gamma_\varphi/M_\varphi = 0.5\text{--}25\%$. In the GW-2HDM, $g_{\varphi t\bar{t}} = \tan\beta$. For the CP -odd case, $\varphi = A$, with $400\text{ GeV} < M_A < 500\text{ GeV}$ and all Γ_A/M_A considered, the region $\tan\beta < 0.50$ was not excluded.³⁶ This is possibly due to an excess at 400 GeV that corresponds to a global (local) significance of 1.9 (3.5 ± 0.3) σ for $\Gamma_A/M_A \simeq 4\%$. The CMS paper noted that higher-order electroweak corrections to SM $gg \rightarrow t\bar{t}$ threshold production may account for the excess and that further improvement in the theoretical description was needed.

To ameliorate the effects of interference of the $gg \rightarrow A/H_2 \rightarrow t\bar{t}$ signal with SM $t\bar{t}$ production, CMS [36] and ATLAS [37] searched for $gg \rightarrow t\bar{t}$ with A/H_2 radiated from one of the top-quarks and decaying to $t\bar{t}$. Both experiments used their full Run 2 data sets, 137 fb^{-1} and 139 fb^{-1} . For these data sets, the interference with SM four-top production was stated to be negligible. In this approach the experiments searched for a

³⁴Decays such as this one were discussed in the one-loop approximation of the GW-2HDM in Refs. [10, 41, 11].

³⁵To our knowledge, this search has not been carried out; nor has one for $H_2 \rightarrow ZA \rightarrow \ell^+\ell^-t\bar{t}$. This decay has a more restricted allowed range; it is discussed below in item 3.

³⁶The same appears to be true for $\varphi = H_2$ with $\Gamma_{H_2}/M_{H_2} \gtrsim 1\%$.

resonant $t\bar{t}$ excess in the four-top-quark data. They expressed 95% CL upper limits on the signal cross section times $B(A/H_2 \rightarrow t\bar{t})$ in terms of the type-II 2HDM of Ref. [12]. In that model, the coupling of A and H_2 is proportional $M_t \cot \beta/v$, and the experiments converted the $\sigma \cdot B$ limits into lower limits on $\tan \beta$. In the GW-2HDM, these translate into upper limits on $\tan \beta$.³⁷ For CMS they are $\tan \beta < 1.6$ (0.7) assuming $M_A = M_{H_2} = 400$ GeV (assuming only H_2 with $M_{H_2} = 600$ GeV); for ATLAS, they are $\tan \beta < 1.7$ (0.9) for $M_A = M_{H_2} = 400$ GeV ($M_{H_2} = 600$ GeV). These limits are much weaker than $\tan \beta < 0.50$ from the earlier CMS and ATLAS searches for $gg \rightarrow H^\pm t\bar{b}$. On the other hand, these four-top searches for a relatively low-mass A or H_2 may benefit substantially from the High Luminosity LHC.

3.) $gg \rightarrow H_2 \rightarrow ZA$

There have been three published searches for $H_2 \rightarrow ZA$ with $ZA \rightarrow \ell^+ \ell^- \bar{b}b$, where $\ell = e$ or μ : [43, 44, 45]. The latter ATLAS search updated the former one with the full Run 2 data set. As with $gg \rightarrow H_2 \rightarrow W^\pm H^\mp$, these H_2 decay rates are proportional to p_Z^3 . They were discussed in the one-loop approximation and two comparisons to the GW-2HDM were presented in Refs. [10, 11]. Two examples were presented, one of which (with $M_{H_2} = 500$ GeV, $M_A = 300$ GeV and $\tan \beta = 0.50$) was excluded at the 95% CL in the newer ATLAS search.

Another approach, without the large $b\bar{b}$ background, is to use $A \rightarrow t\bar{t}$. In the two-loop perturbative method, the region $M_A = 350\text{--}365$ GeV corresponds to $M_{H_2} = 630$ GeV down to 508 GeV and has substantial ($> 20\%$) branching ratios of $H_2 \rightarrow ZA$. In the amoeba method, there is no $M_{H_2} > M_A + 100$ TeV for which $M_A > 2M_t$. It's worth a try; nothing ventured, nothing gained.

³⁷See the note below Eq. (4) in Sec. I.

Acknowledgments

EE thanks the Fermi Research Alliance, LLC under Contract No. DE-AC02-07CH11359 with the U. S. Department of Energy, Office of Science, Office of High Energy Physics. KL thanks Laboratoire d'Annecy-le-Vieux de Physique Théorique (LAPTh) for its hospitality during the final stage of this work. We are very grateful for valuable guidance from Stephen Martin. We also thank Kevin Black, Jon Butterworth, Alvaro De Rujula, Ulrich Heintz, Guoan Hu, and William John Murray for many helpful discussions and suggestions.

References

- [1] E. Gildener and S. Weinberg, “Symmetry Breaking and Scalar Bosons,” *Phys. Rev.* **D13** (1976) 3333.
- [2] F. Boudjema and A. Semenov, “Measurements of the SUSY Higgs selfcouplings and the reconstruction of the Higgs potential,” *Phys. Rev. D* **66** (2002) 095007, hep-ph/0201219.
- [3] J. F. Gunion and H. E. Haber, “The CP conserving two Higgs doublet model: The Approach to the decoupling limit,” *Phys. Rev.* **D67** (2003) 075019, hep-ph/0207010.
- [4] M. Carena, I. Low, N. R. Shah, and C. E. M. Wagner, “Impersonating the Standard Model Higgs Boson: Alignment without Decoupling,” *JHEP* **04** (2014) 015, 1310.2248.
- [5] P. Draper, A. Ekstedt, and H. E. Haber, “A natural mechanism for approximate Higgs alignment in the 2HDM,” *JHEP* **05** (2021) 235, 2011.13159.
- [6] H. E. Haber and J. P. Silva, “Exceptional regions of the 2HDM parameter space,” *Phys. Rev. D* **103** (2021), no. 11, 115012, 2102.07136.

- [7] S. R. Coleman and E. J. Weinberg, “Radiative Corrections as the Origin of Spontaneous Symmetry Breaking,” *Phys. Rev.* **D7** (1973) 1888–1910.
- [8] K. Lane and W. Shepherd, “Natural stabilization of the Higgs boson’s mass and alignment,” *Phys. Rev.* **D99** (2019), no. 5, 055015, 1808.07927.
- [9] B. Bellazzini, C. Csaki, J. Hubisz, J. Serra, and J. Terning, “A Higgslike Dilaton,” *Eur. Phys. J.* **C73** (2013), no. 2, 2333, 1209.3299.
- [10] K. Lane and E. Pilon, “Phenomenology of the new light Higgs bosons in Gildener-Weinberg models,” *Phys. Rev. D* **101** (2020), no. 5, 055032, 1909.02111.
- [11] E. J. Eichten and K. Lane, “Higgs alignment and the top quark,” *Phys. Rev. D* **103** (2021), no. 11, 115022, 2102.07242.
- [12] G. C. Branco, P. M. Ferreira, L. Lavoura, M. N. Rebelo, M. Sher, and J. P. Silva, “Theory and phenomenology of two-Higgs-doublet models,” *Phys. Rept.* **516** (2012) 1–102, 1106.0034.
- [13] S. P. Martin, “Two Loop Effective Potential for a General Renormalizable Theory and Softly Broken Supersymmetry,” *Phys. Rev.* **D65** (2002) 116003, hep-ph/0111209.
- [14] R. A. Battye, G. D. Brawn, and A. Pilaftsis, “Vacuum Topology of the Two Higgs Doublet Model,” *JHEP* **08** (2011) 020, 1106.3482.
- [15] A. Pilaftsis, “On the Classification of Accidental Symmetries of the Two Higgs Doublet Model Potential,” *Phys. Lett.* **B706** (2012) 465–469, 1109.3787.
- [16] J. S. Lee and A. Pilaftsis, “Radiative Corrections to Scalar Masses and Mixing in a Scale Invariant Two Higgs Doublet Model,” *Phys. Rev.* **D86** (2012) 035004, 1201.4891.
- [17] S. L. Glashow and S. Weinberg, “Natural Conservation Laws for Neutral Currents,” *Phys. Rev.* **D15** (1977) 1958.

- [18] **Particle Data Group** Collaboration, R. L. Workman, “Review of Particle Physics,” *PTEP* **2022** (2022) 083C01.
- [19] **CMS** Collaboration, V. Khachatryan *et. al.*, “Search for a charged Higgs boson in pp collisions at $\sqrt{s} = 8$ TeV,” *JHEP* **11** (2015) 018, 1508.07774.
- [20] **ATLAS** Collaboration, M. Aaboud *et. al.*, “Search for charged Higgs bosons decaying into top and bottom quarks at $\sqrt{s} = 13$ TeV with the ATLAS detector,” *JHEP* **11** (2018) 085, 1808.03599.
- [21] R. Jackiw, “Functional evaluation of the effective potential,” *Phys. Rev. D* **9** (1974) 1686.
- [22] S. R. Coleman and S. L. Glashow, “Departures from the eightfold way: Theory of strong interaction symmetry breakdown,” *Phys. Rev.* **134** (1964) B671–B681.
- [23] S. Coleman, “Notes from Sidney Coleman’s Physics 253a: Quantum Field Theory,” 1110.5013.
- [24] W. H. Press, S. A. Teukolsky, W. T. Vetterling, and B. P. Flannery, *Numerical Recipes in C*. Cambridge University Press, Cambridge, USA, second ed., 1992.
- [25] J. Braathen, S. Kanemura, and M. Shimoda, “Two-loop analysis of classically scale-invariant models with extended Higgs sectors,” *JHEP* **03** (2021) 297, 2011.07580.
- [26] S. Heinemeyer, C. Li, F. Lika, G. Moortgat-Pick, and S. Paasch, “A 96 GeV Higgs Boson in the 2HDM plus Singlet,” 2112.11958.
- [27] **ATLAS** Collaboration, “A detailed map of Higgs boson interactions by the ATLAS experiment ten years after the discovery,” *Nature* **607** (2022), no. 7917, 52–59, 2207.00092.
- [28] **CMS** Collaboration, “A portrait of the Higgs boson by the CMS experiment ten years after the discovery,” *Nature* **607** (2022), no. 7917, 60–68, 2207.00043.

- [29] S. L. Glashow, “Partial Symmetries of Weak Interactions,” *Nucl. Phys.* **22** (1961) 579–588.
- [30] S. Weinberg, “A Model of Leptons,” *Phys.Rev.Lett.* **19** (1967) 1264–1266.
- [31] F. Englert and R. Brout, “Broken Symmetry and the Mass of Gauge Vector Mesons,” *Phys.Rev.Lett.* **13** (1964) 321–323.
- [32] P. W. Higgs, “Broken symmetries, massless particles and gauge fields,” *Phys.Lett.* **12** (1964) 132–133.
- [33] G. Guralnik, C. Hagen, and T. Kibble, “Global Conservation Laws and Massless Particles,” *Phys.Rev.Lett.* **13** (1964) 585–587.
- [34] **ATLAS** Collaboration, G. Aad *et. al.*, “Observation of a new particle in the search for the Standard Model Higgs boson with the ATLAS detector at the LHC,” *Phys.Lett.* **B716** (2012) 1–29, 1207.7214.
- [35] **CMS** Collaboration, S. Chatrchyan *et. al.*, “Observation of a new boson at a mass of 125 GeV with the CMS experiment at the LHC,” *Phys.Lett.* **B716** (2012) 30–61, 1207.7235.
- [36] **CMS** Collaboration, A. M. Sirunyan *et. al.*, “Search for production of four top quarks in final states with same-sign or multiple leptons in proton-proton collisions at $\sqrt{s} = 13$ TeV,” *Eur. Phys. J. C* **80** (2020), no. 2, 75, 1908.06463.
- [37] **ATLAS** Collaboration, “Search for $t\bar{t}H/A \rightarrow t\bar{t}\bar{t}\bar{t}$ production in the multilepton final state in proton-proton collisions at $\sqrt{s} = 13$ TeV with the ATLAS detector, ATLAS-CONF-2022-008,”.
- [38] **CMS** Collaboration, A. M. Sirunyan *et. al.*, “Search for a charged Higgs boson decaying into top and bottom quarks in events with electrons or muons in proton-proton collisions at $\sqrt{s} = 13$ TeV,” *JHEP* **01** (2020) 096, 1908.09206.

- [39] **ATLAS** Collaboration, G. Aad *et. al.*, “Search for charged Higgs bosons decaying into a top quark and a bottom quark at $\sqrt{s} = 13$ TeV with the ATLAS detector,” *JHEP* **06** (2021) 145, 2102.10076.
- [40] **CMS** Collaboration, A. M. Sirunyan *et. al.*, “Search for charged Higgs bosons decaying into a top and a bottom quark in the all-jet final state of pp collisions at $\sqrt{s} = 13$ TeV,” *JHEP* **07** (2020) 126, 2001.07763.
- [41] G. Brooijmans *et. al.*, “Les Houches 2019 Physics at TeV Colliders: New Physics Working Group Report,” in *11th Les Houches Workshop on Physics at TeV Colliders: PhysTeV Les Houches. 2*, 2020. 2002.12220.
- [42] **CMS** Collaboration, A. M. Sirunyan *et. al.*, “Search for heavy Higgs bosons decaying to a top quark pair in proton-proton collisions at $\sqrt{s} = 13$ TeV,” *JHEP* **04** (2020) 171, 1908.01115.
- [43] **ATLAS** Collaboration, M. Aaboud *et. al.*, “Search for a heavy Higgs boson decaying into a Z boson and another heavy Higgs boson in the $\ell\ell b\bar{b}$ final state in pp collisions at $\sqrt{s} = 13$ TeV with the ATLAS detector,” *Phys. Lett.* **B783** (2018) 392–414, 1804.01126.
- [44] **CMS** Collaboration, A. M. Sirunyan *et. al.*, “Search for new neutral Higgs bosons through the $H \rightarrow ZA \rightarrow \ell^+ \ell^- b\bar{b}$ process in pp collisions at $\sqrt{s} = 13$ TeV,” *JHEP* **03** (2020) 055, 1911.03781.
- [45] **ATLAS** Collaboration, G. Aad *et. al.*, “Search for a heavy Higgs boson decaying into a Z boson and another heavy Higgs boson in the $\ell\ell b\bar{b}$ and $\ell\ell WW$ final states in pp collisions at $\sqrt{s} = 13$ TeV with the ATLAS detector,” *Eur. Phys. J. C* **81** (2021), no. 5, 396, 2011.05639.